JCI The Journal of Clinical Investigation

Dynamin 2 regulates biphasic insulin secretion and plasma glucose homeostasis

Fan Fan, … , Louis H. Philipson, Xuelin Lou

J Clin Invest. 2015;125(11):4026-4041. https://doi.org/10.1172/JCI80652.

Research Article **Endocrinology**

Alterations in insulin granule exocytosis and endocytosis are paramount to pancreatic β cell dysfunction in diabetes mellitus. Here, using temporally controlled gene ablation specifically in β cells in mice, we identified an essential role of dynamin 2 GTPase in preserving normal biphasic insulin secretion and blood glucose homeostasis. Dynamin 2 deletion in β cells caused glucose intolerance and substantial reduction of the second phase of glucose-stimulated insulin secretion (GSIS); however, mutant β cells still maintained abundant insulin granules, with no signs of cell surface expansion. Compared with control β cells, real-time capacitance measurements demonstrated that exocytosis-endocytosis coupling was less efficient but not abolished; clathrin-mediated endocytosis (CME) was severely impaired at the step of membrane fission, which resulted in accumulation of clathrin-coated endocytic intermediates on the plasma membrane. Moreover, dynamin 2 ablation in β cells led to striking reorganization and enhancement of actin filaments, and insulin granule recruitment and mobilization were impaired at the later stage of GSIS. Together, our results demonstrate that dynamin 2 regulates insulin secretory capacity and dynamics in vivo through a mechanism depending on CME and F-actin remodeling. Moreover, this study indicates a potential pathophysiological link between endocytosis and diabetes mellitus.

Dynamin 2 regulates biphasic insulin secretion and plasma glucose homeostasis

Fan Fan,[1] Chen Ji,[1] Yumei Wu,[2] Shawn M. Ferguson,[2] Natalia Tamarina,[3] Louis H. Philipson,[3] and Xuelin Lou[1]

[1]Department of Neuroscience, School of Medicine and Public Health, University of Wisconsin-Madison, Madison, Wisconsin, USA. [2]Department of Cell Biology, Program in Cellular Neuroscience, Neurodegeneration and Repair, Yale University School of Medicine, New Haven, Connecticut, USA. [3]Department of Medicine, Kovler Diabetes Center, University of Chicago, Chicago, Illinois, USA.

Alterations in insulin granule exocytosis and endocytosis are paramount to pancreatic β cell dysfunction in diabetes mellitus. Here, using temporally controlled gene ablation specifically in β cells in mice, we identified an essential role of dynamin 2 GTPase in preserving normal biphasic insulin secretion and blood glucose homeostasis. Dynamin 2 deletion in β cells caused glucose intolerance and substantial reduction of the second phase of glucose-stimulated insulin secretion (GSIS); however, mutant β cells still maintained abundant insulin granules, with no signs of cell surface expansion. Compared with control β cells, real-time capacitance measurements demonstrated that exocytosis-endocytosis coupling was less efficient but not abolished; clathrin-mediated endocytosis (CME) was severely impaired at the step of membrane fission, which resulted in accumulation of clathrin-coated endocytic intermediates on the plasma membrane. Moreover, dynamin 2 ablation in β cells led to striking reorganization and enhancement of actin filaments, and insulin granule recruitment and mobilization were impaired at the later stage of GSIS. Together, our results demonstrate that dynamin 2 regulates insulin secretory capacity and dynamics in vivo through a mechanism depending on CME and F-actin remodeling. Moreover, this study indicates a potential pathophysiological link between endocytosis and diabetes mellitus.

Introduction

Proper regulation of membrane trafficking balances material and signal exchange and is fundamental to cellular functions. Similar to nerve terminals, in which endocytosis supports high rates of synaptic vesicle recycling (1, 2), neuroendocrine cells undergo vigorous membrane trafficking to regulate large dense-core vesicle (LDCV) release and cellular functions. However, the mechanisms by which endocytosis influences secretory function are unclear, and the molecular nature of endocytosis in these cells remains poorly understood. Pancreatic β cells are the only cell type that releases insulin in humans. Failure of insulin secretion due to β cell loss or functional decline causes type 1 diabetes and type 2 diabetes (T2D), respectively (3). Declines in insulin secretion may arise from the defects of single or multiple steps in the insulin granule trafficking cycle, including granule biogenesis from the trans-Golgi network (TGN), subsequent maturation, recruitment to the plasma membrane (PM), exocytosis, endocytosis, and endosome-to-TGN traffic. It is imperative to understand how regulated membrane trafficking controls insulin secretion.

In response to continuous exposure to high concentrations of glucose, insulin release proceeds in two distinct temporal phases in both humans (4) and rodents (5, 6), including a fast, transient first phase and a slow, sustained second phase. In patients with T2D, the second phase is strongly reduced and the first phase is nearly abolished (7). Multiple factors contribute to the biphasic nature of glucose-stimulated insulin secretion (GSIS), including distinct pools of insulin granules, metabolic signaling, and actin cytoskeleton remodeling (8–12). The granules docked to the PM, also known as the readily releasable pool (RRP) granules, mainly contribute to the first phase. Direct total internal reflection fluorescence (TIRF) imaging suggests that the granules near the PM participate in the first phase and the "newcomer" granules mobilized from a reserve pool located a distance away from the PM produce the second phase of GSIS (12). Moreover, increasing evidence supports an emerging model in which the actin cytoskeleton plays a critical role in biphasic GSIS (10, 11) through granule mobilization and recruitment from the reserve pool to the PM. Many actin remodeling molecules, such as the Rho GTPase family proteins Cdc42 (13) and RAC1 (14), PAK1 (15), N-WASP (16), and PPARβ/δ (17), selectively regulate the second phase of GSIS, and perturbations of microtubules (18) and kinesin-1 (19) disrupt the second phase.

Upon glucose stimulation, β cells rapidly uptake glucose and generate ATP, which closes $K_{(ATP)}$ channels and depolarizes the PM, and the subsequent intracellular Ca^{2+} increase triggers insulin granule exocytosis (3, 20). After exocytosis, the membrane components of insulin granules (such as lipids, v-SNAREs, synaptotagmin, transporters, and ATPases, etc.) are internalized and transported to the TGN in order to complete the cycle of granule membrane trafficking. The exocytosis-endocytosis coupling of insulin granules was first demonstrated by a pioneering electron microscopy (EM) study in 1973 (21). Since then, the study of β cell endocytosis has been largely stalled, in sharp contrast to the remarkable progress made in characterizing insulin exocytosis at both molecular and cellular levels. Individual insulin granules have two fates after fusion with the PM: pinching off intact following a transient fusion pore opening (termed "kiss and run," refs. 22, 23, and/or "cavicapture," ref. 24) or being retrieved through undefined mechanisms after a full collapse onto the PM. Mem-

Conflict of interest: The authors have declared that no conflict of interest exists.
Submitted: December 29, 2014; **Accepted:** August 20, 2015.
Reference information: *J Clin Invest*. 2015;125(11):4026–4041. doi:10.1172/JCI80652.

brane capacitance studies in β cells demonstrate heterogeneous endocytosis kinetics and different endocytosis modulation by Ca^{2+} (25, 26), IP_6 (27), G proteins (28), and actin (26). However, the molecular nature of endocytosis machinery in β cells is poorly understood, and how endocytosis regulates β cell function and glucose homeostasis in vivo is unknown.

Dynamin was originally identified as a microtubule-binding GTPase (29) and later identified as a pinchase to free endocytic vesicles from the PM (refs. 30, 31, and for review, see refs. 32, 33). In *shibire* mutants of *Drosophila*, nearly empty nerve terminals at a nonpermissive temperature after stimulation (34) suggest an essential role of dynamin in synaptic vesicle reformation. In mammals, dynamin is encoded by 3 genes (32): *Dnm1*, *Dnm2*, and *Dnm3*. Dynamin 1 is highly expressed in the nervous system, dynamin 2 is ubiquitous in all tissues, and dynamin 3 is found primarily in neuronal tissues and at low levels in testis (35, 36). At nerve terminals, dynamin 1 and 3 contribute to synaptic vesicle reformation and neurotransmission (36–40); synapses lacking dynamin 1 (and dynamin 3) have fewer vesicles and abundant clathrin-coated profiles (CCPs) accumulated on the PM (36, 38, 40). In nonneuronal cells, dynamin isoforms appear cell-type specific and may play distinct roles in multiple endocytosis pathways (32, 35, 41). Recent studies further highlighted the diverse functions of dynamin in other biological processes (42–44).

Here, we studied dynamin 2 function in insulin secretion and glucose homeostasis in vivo. We generated tamoxifen-inducible β cell–specific *Dnm2* KO mice. The KO mice developed significant glucose intolerance and a pronounced reduction of the second phase of GSIS. β Cells lacking dynamin 2 contained abundant insulin granules, as did controls, but the clathrin-mediated endocytosis (CME) was strongly impaired at the later stage of membrane retrievals. Moreover, KO cells exhibited striking reorganization and enhancement in cortical F-actin, which can be fully rescued by reexpressing dynamin in these cells; TIRF imaging at single-cell levels revealed selective reduction of insulin secretion and granule recruitment at the later stage of glucose stimulation. These data provide direct genetic evidence that dynamin 2 regulates biphasic insulin secretion and glucose homeostasis in mammals, implying a potential link between dynamin 2–mediated membrane trafficking and the pathogenesis of diabetes mellitus.

Results

Pancreatic β cells express multiple dynamin isoforms. Western blots of purified pancreatic islets revealed that dynamin 2 was abundant and dynamin 1 was not detectable (Figure 1, A–C, and Supplemental Figure 1, A and B; supplemental material available online with this article; doi:10.1172/JCI80652DS1). Interestingly, we found fairly rich levels of dynamin 3 (Figure 1C), which is reported primarily in neuronal tissues and at low levels in testis (35). The antibody specificity was verified using cell lysates from tissues with appropriate dynamin genotypes as negative and positive controls. Immunohistochemistry of pancreatic sections showed strong dynamin 2 (but not dynamin 1) fluorescence in islets (Figure 1, D and E) and low levels of dynamin 3 distributed equally in islets and exocrine areas of pancreas (Figure 1F). Immunocytochemistry of isolated individual β cells in cultures confirmed the coexpression of dynamin 2 and 3 in β cells (Supplemental Figure 1C). The dynamin 2 fluorescence was punctate at the PM (Figure 1G) but was more diffuse throughout cytosol, with a slightly enhanced signal in some perinuclear regions (Supplemental Figure 2, B and C). Dynamin 2 signal was largely separated from insulin granules, with only a limited number of dynamin 2 puncta colocalized with granules (Figure 1G).

Temporally controlled dynamin 2 deletion in pancreatic β cells impairs glucose homeostasis in vivo. To study dynamin 2 function in β cells at both cellular and whole organism levels, we generated the *Dnm2* KO mouse model, in which dynamin deletion was temporally controlled and limited in β cells. To this end, we crossed $Dnm2^{fl/fl}$ mice (45) with *Tg(Ins1-Cre/ERT)1Lphi* (also termed *MIP1-CreERT*) transgenic mice (46) that selectively express Cre estrogen receptor fusion proteins driven by a mouse insulin-1 promoter (*Ins1*) in β cells. The latter has improved β cell selectivity (no ectopic expression in hypothalamus in the brain) compared with other β cell *Cre* or *CreERT* lines (47). After tamoxifen treatment, Cre recombinase translocated from the cytosol into nuclei and deleted the *Dnm2* gene in β cells (Figure 2A). *Dnm2* KO mice were viable and not grossly distinguishable from their littermate controls. Western blotting and immunohistochemistry experiments (Figure 2, B and C) demonstrated markedly lower levels of dynamin 2 in KO islets than in control islets, indicating efficient dynamin 2 depletion. The remaining fluorescence was presumably from the non–β cells in pancreatic islets, such as α, δ, and pancreatic polypeptide cells, or weak background fluorescence from β cells. We often saw some α cells in the center of KO islets, in contrast to the periphery distribution of α cells in control islets (Supplemental Figure 3). The dynamin 2 deletion, specifically in β cells but not in α cells, was confirmed (Supplemental Figure 4), consistent with the β cell–specific expression of Cre recombinase in *MIP1-CreERT* mice (46, 47).

We first examined how dynamin 2 deletion influences glucose homeostasis at the system level in vivo. The *Dnm2* KO mice exhibited significant glucose intolerance following glucose administration (i.p.) compared with their littermate controls without *MIP1-CreERT* (Figure 2E), in spite of their similar body weights (Figure 2D). Further experiments in vehicle-treated $Dnm2^{fl/fl}$ *MIP1-CreERT* mice and $Dnm2^{fl/fl}$ mice showed no significant difference between different control groups. The AUC of glucose levels in KO mice was significantly higher than different controls (Figure 2F; $P = 0.039$, 1-way ANOVA). These data demonstrated the glucose intolerance observed in *Dnm2* KO mice was caused by a direct dynamin 2 deletion in β cells rather than other nonspecific factors, such as gene background or tamoxifen treatment itself. Moreover, the glucose intolerance was further exacerbated by metabolic stress induced by high-fat feeding for 3 months (Figure 2, I and J). However, KO mice had similar body weight compared with that of their littermate controls (Figure 2, D and H), and the insulin sensitivity in KO mice remained normal in both physiologically and metabolically stressed conditions (Figure 2, G and K).

To further verify glucose homeostasis deficiency in dynamin 2 KO mice, we monitored plasma glucose responses following 3 glucose injections (i.p., every 30 minutes) (Figure 2, L–N). Different control groups had a comparable body weights and responded similarly to glucose stimulation. They maintained a plateau level of glucose, without further significant increase at 30 minutes after the first injection (Figure 2M), indicating a strong capacity of glucose handling in vivo to stabilize healthy levels of plasma glucose,

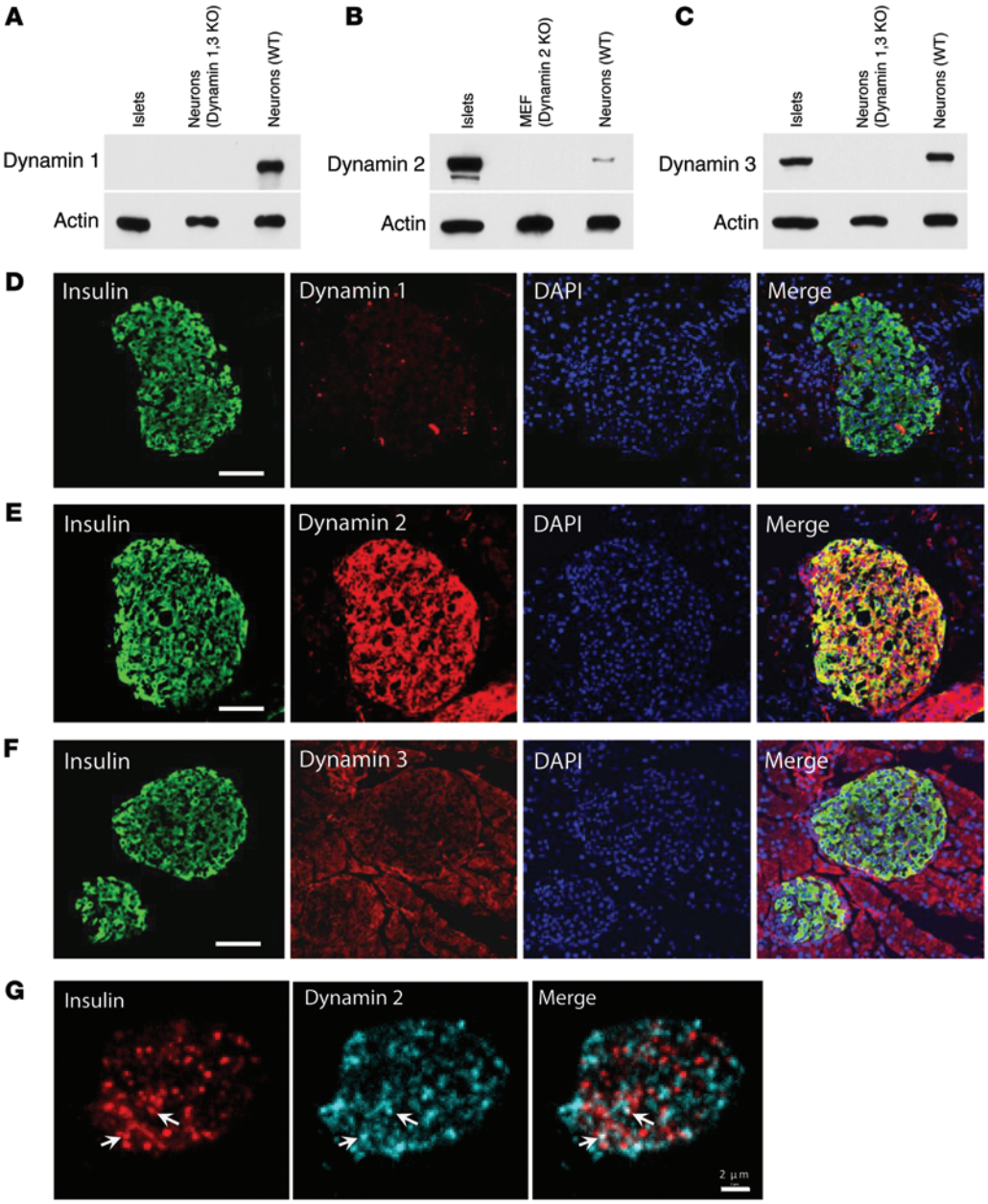

Figure 1. Dynamin isoforms in mouse pancreatic islets. (**A**–**C**) Western blots for dynamin 1, 2, and 3 in purified mouse islet lysate (lane 1). The specificity of antibodies was verified using cell lysates with the indicated dynamin genotype as positive and negative controls (lanes 2 and 3). 110–150 islets were used for each lane. Each panel shows representative results from 3 to 5 independent experiments. MEF, mouse embryo fibroblasts. (**D**–**F**) Immunofluorescence of dynamin 1, 2, and 3 in mouse pancreatic islets. (**G**) Subcellular distribution of dynamin 2 in β cells (bottom optical section using spinning disk confocal microscopy views). Arrows indicate dynamin 2 puncta colocalized with insulin granules. Scale bars: 50 μm (**D**–**F**); 2 μm (**G**).

even after strong glucose challenge. KO mice had significantly higher levels of plasma glucose than all control groups after injections (Figure 2, M and N), despite the fact that they responded with a similar plateau-increase pattern. This suggests a defect in continuous insulin secretion and glucose handling capacity during the prolonged glucose stimulation. The AUC in KO mice was significantly higher than that in controls (Figure 2N, $P = 0.003$, 1-way ANOVA). In summary, these in vivo experiments revealed a specific role of dynamin 2 in glucose homeostasis at the system level; the intact insulin sensitivity excludes a potential defect in insulin signaling in peripheral tissues of KO mice, pointing to insufficient insulin release from pancreatic β cells.

Dynamin 2 is essential for preserving normal biphasic insulin release. Next, we examined dynamin 2 function in biphasic GSIS by direct secretion measurement from pancreatic islets. The continuous glucose (20 mM) stimulation induced a typical biphasic pattern of insulin release in control islets (Figure 3A). The first phase peaked at approximately 5 minutes after stimulation and deceased within the following 5~10 minutes; the second phase was relatively slow and long lasting. Such biphasic GSIS in control islets closely mimicked insulin release in vivo, as demonstrated in awake mice under hyperglycemic clamp (6). However, GSIS in KO mice was markedly decreased in the second phase (Figure 3A). Interestingly, the first phase of GSIS in KO islets reached a comparable peak amplitude at a time similar to that in controls and then decreased faster. Insulin secretion induced by 30 mM KCl showed similar properties, with comparable kinetics and peak amplitude for both groups (Figure 3B). The AUC analysis showed that insulin secretion in the second phase (20–40 minutes) in KO mice was significantly lower than that of controls (Figure 3D, $P = 0.0051$); insulin secretion in the first phase (10–20 minutes) and during 30 mM KCl stimulation decreased only slightly (Figure 3, C and E;

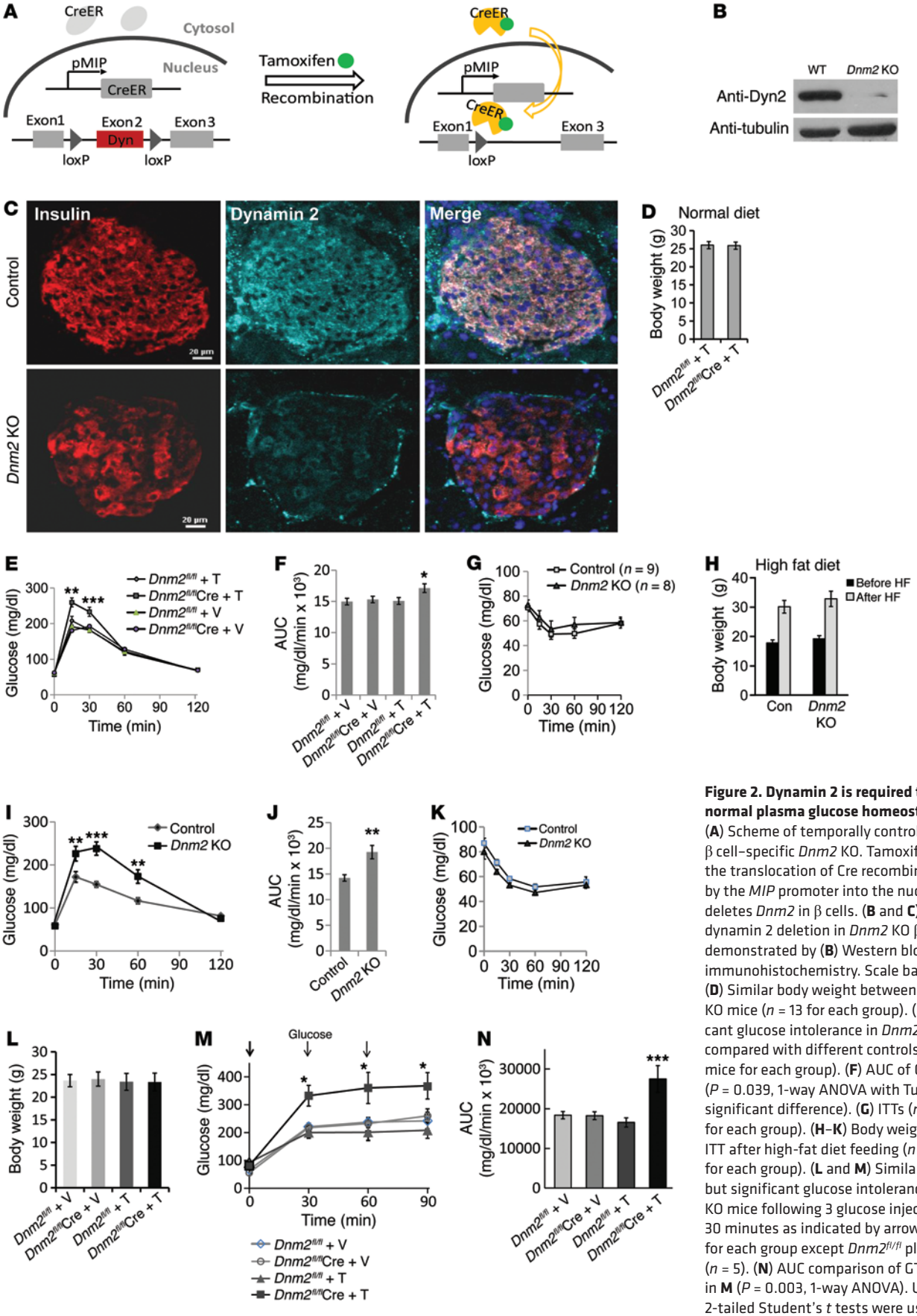

Figure 2. Dynamin 2 is required to maintain normal plasma glucose homeostasis in vivo. (**A**) Scheme of temporally controlled, β cell–specific *Dnm2* KO. Tamoxifen triggers the translocation of Cre recombinase driven by the *MIP* promoter into the nucleus and deletes *Dnm2* in β cells. (**B** and **C**) Efficient dynamin 2 deletion in *Dnm2* KO β cells demonstrated by (**B**) Western blots and (**C**) immunohistochemistry. Scale bar: 20 μm. (**D**) Similar body weight between control and KO mice (n = 13 for each group). (**E**) Significant glucose intolerance in *Dnm2* KO mice compared with different controls (n = 11–13 mice for each group). (**F**) AUC of GTT curves (P = 0.039, 1-way ANOVA with Tukey honest significant difference). (**G**) ITTs (n = 8–9 mice for each group). (**H**–**K**) Body weight, GTT, and ITT after high-fat diet feeding (n = 6–8 mice for each group). (**L** and **M**) Similar body weight but significant glucose intolerance in *Dnm2* KO mice following 3 glucose injections (every 30 minutes as indicated by arrows); n = 6 mice for each group except $Dnm2^{fl/fl}$ plus tamoxifen (n = 5). (**N**) AUC comparison of GTT curves in **M** (P = 0.003, 1-way ANOVA). Unpaired 2-tailed Student's t tests were used unless specified. T, tamoxifen; V, vehicle. $^*P < 0.05$, $^{**}P < 0.01$, $^{***}P < 0.005$.

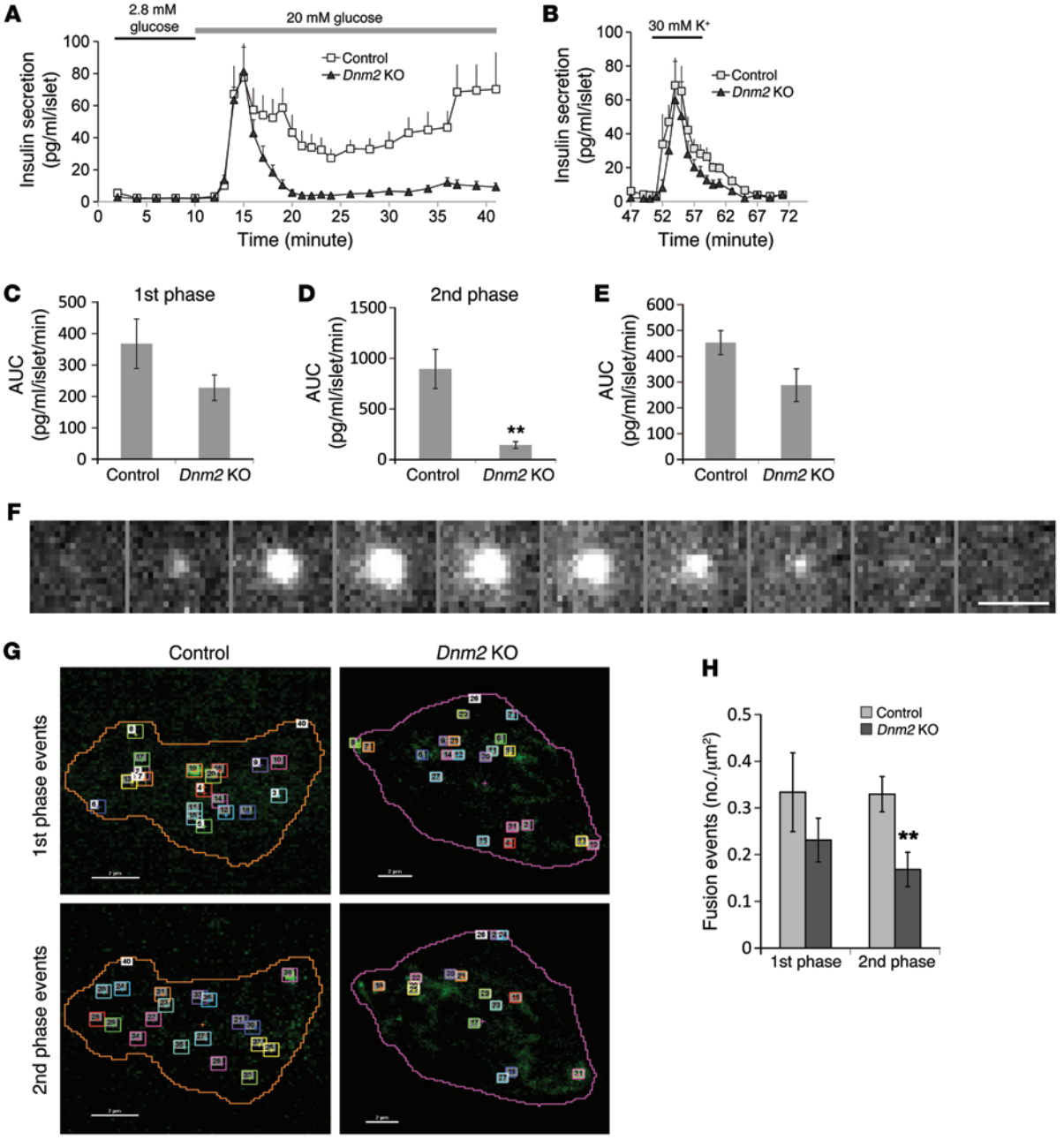

Figure 3. Dynamin 2 regulates biphasic insulin secretion induced by 20 mM glucose. (**A**) 20 mM glucose induced biphasic insulin secretion from both control and *Dnm2* KO islets (n = 5 independent experiments for each group, n = 30–50 islets per experiment per genotype). (**B**) 30 mM KCl induced insulin secretion after 10 minutes rest from the same islet samples in **A**. (**C** and **D**) AUC analysis for the first phase (10–20 minutes, n = 5 each; P = 0.17, 2-tailed t test) and the second phase (20–40 minutes, n = 5 each, P = 0.016, 2-tailed t test) of GSIS shown in **A**. (**E**) AUC analysis of insulin secretion (P = 0.07, 2-tailed t test) induced by 30 mM KCl from **B**. (**F**) Time-lapse live-cell TIRFM of a representative fusion event in a control β cell expressing NPY-pHluorin (20 Hz). (**G**) Total granule fusion events under TIRFM during the first phase (during the first 0–6 minutes) and the second phase (during minutes 7–20) of GSIS under 20 mM glucose stimulation. Each square in the images marked a single fusion event. (**H**) The average number of fusion events in the first phase (n = 8 and 14 for control and KO cells, respectively; P = 0.30, 2-tailed t test) and second phase of GSIS (n = 7 and 6 for control and KO cells, respectively; P = 0.01, 2-tailed t test). Scale bars: 1 μm (**F**); 2 μm (**G**). $^{**}P < 0.01$.

P = 0.07, n = 5 independent experiments), which may indicate some subtle defects in insulin secretion from the RRP. Thus, dynamin 2 regulates biphasic insulin secretion, with much greater impact on the second phase of GSIS than the first phase.

We next examined insulin granule fusion in individual β cells using TIRF microscopy (TIRFM). We generated NPY-pHluorin, a pH-sensitive fluorescent probe that selectively targets in insulin granules and shows strong fluorescence only in nonacidic environment, to sensitively detect insulin granule fusion. Each fusion event can be readily identified by transient brightening of fluorescent spots due to the pH increase in the granules upon fusion with the PM, and the signal-to-noise ratio of fluorescence is very high

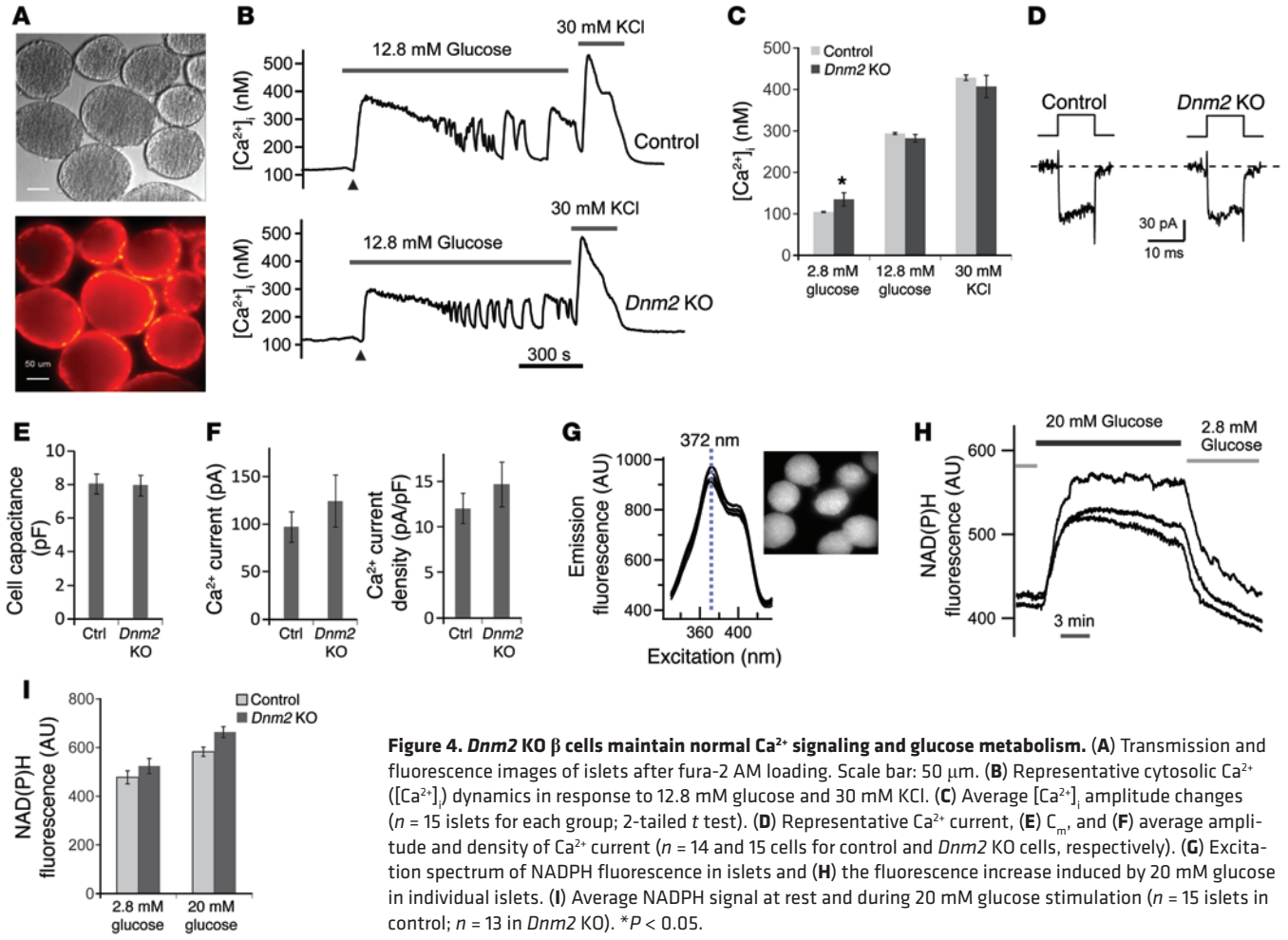

Figure 4. *Dnm2* KO β cells maintain normal Ca^{2+} signaling and glucose metabolism. (**A**) Transmission and fluorescence images of islets after fura-2 AM loading. Scale bar: 50 μm. (**B**) Representative cytosolic Ca^{2+} ($[Ca^{2+}]_i$) dynamics in response to 12.8 mM glucose and 30 mM KCl. (**C**) Average $[Ca^{2+}]_i$ amplitude changes (n = 15 islets for each group; 2-tailed t test). (**D**) Representative Ca^{2+} current, (**E**) C_m, and (**F**) average amplitude and density of Ca^{2+} current (n = 14 and 15 cells for control and *Dnm2* KO cells, respectively). (**G**) Excitation spectrum of NADPH fluorescence in islets and (**H**) the fluorescence increase induced by 20 mM glucose in individual islets. (**I**) Average NADPH signal at rest and during 20 mM glucose stimulation (n = 15 islets in control; n = 13 in *Dnm2* KO). *$P < 0.05$.

in our experiments. Figure 3F shows a typical fusion event visualized under TIRFM. During continuous perfusion of 20 mM glucose, individual β cells often responded with a burst of exocytosis events at the beginning, followed by sparse fusion events at later stages. Figure 3G shows the individual fusion events during the first 6 minutes (the first phase) and from minute 7 to minute 20 (the second phase) of 20 mM glucose stimulation in a β cell from control and KO mice. Quantitative analysis (Figure 3H) revealed a significant decrease in the second phase (P = 0.01; n = 8 and 14 cells for control and KO) and only a slight decrease (P = 0.30) in the first phase in KO mice. Thus, dynamin 2 is required to support biphasic insulin release at the single-cell level, in close parallel with the data from intact islet perifusion (Figure 3A).

Dynamin 2 regulates insulin secretion with normal intracellular Ca^{2+} levels and glucose metabolism. Insulin secretion can be regulated at different steps of insulin granule trafficking. We visualized the dynamics of intracellular Ca^{2+} concentration ($[Ca^{2+}]_i$), a key factor frequently implicated in insulin secretion deficiency, during GSIS in intact islets (Figure 4, A–C). 12.8 mM glucose elicited a fast $[Ca^{2+}]_i$ rise for approximately 5 minutes and subsequent $[Ca^{2+}]_i$ oscillations in control islets, and the rises and oscillations all started with a small and transient $[Ca^{2+}]_i$ decrease (Figure 4B, arrowheads). Further, direct KCl (30 mM) stimulation generated a $[Ca^{2+}]_i$ increase with a shorter delay and higher amplitude than glucose stimulation. The $[Ca^{2+}]_i$ properties in KO islets were very similar to those in controls, albeit with slightly higher basal levels. Moreover, in good agreement with the Ca^{2+} imaging data, patch-clamp experiments demonstrated the comparable amplitude and density of Ca^{2+} currents between control and KO β cells (Figure 4, D and F).

We further examined the metabolic status of β cells using NADPH imaging (Figure 4G). NADPH fluorescence in islets showed large heterogeneity from islet to islet (Figure 4H); continuous NADPH fluorescence imaging at basal and glucose stimulation conditions demonstrated normal mitochondrial glucose metabolism in KO islets (Figure 4, H and I). Thus, $[Ca^{2+}]_i$ dynamics, glucose sensing, and mitochondrial metabolism were intact in *Dnm2* KO β cells.

Intact RRP of insulin granules in the absence of dynamin 2 in β cells. The sizes of RRP and the reserve pool of insulin granules are key factors that affect GSIS dynamics in β cells. Next, we investigated insulin granule pool properties using EM. Insulin granules in KO cells were abundant and had similar size (~360 nm in diameter) (Figure 5, A–C) and subcellular spatial distribution as that in controls (Supplemental Figure 5, A–C). The docked granule number, as a morphological estimate of RRP, was comparable between control and KO groups (Figure 5, A, B, and D). Given the proposed dynamin function in endocytosis and vesicle biogenesis from the TGN (48–51), it is interesting that we found no significant decrease in granule density in KO β cells (Figure 5, B and C, and

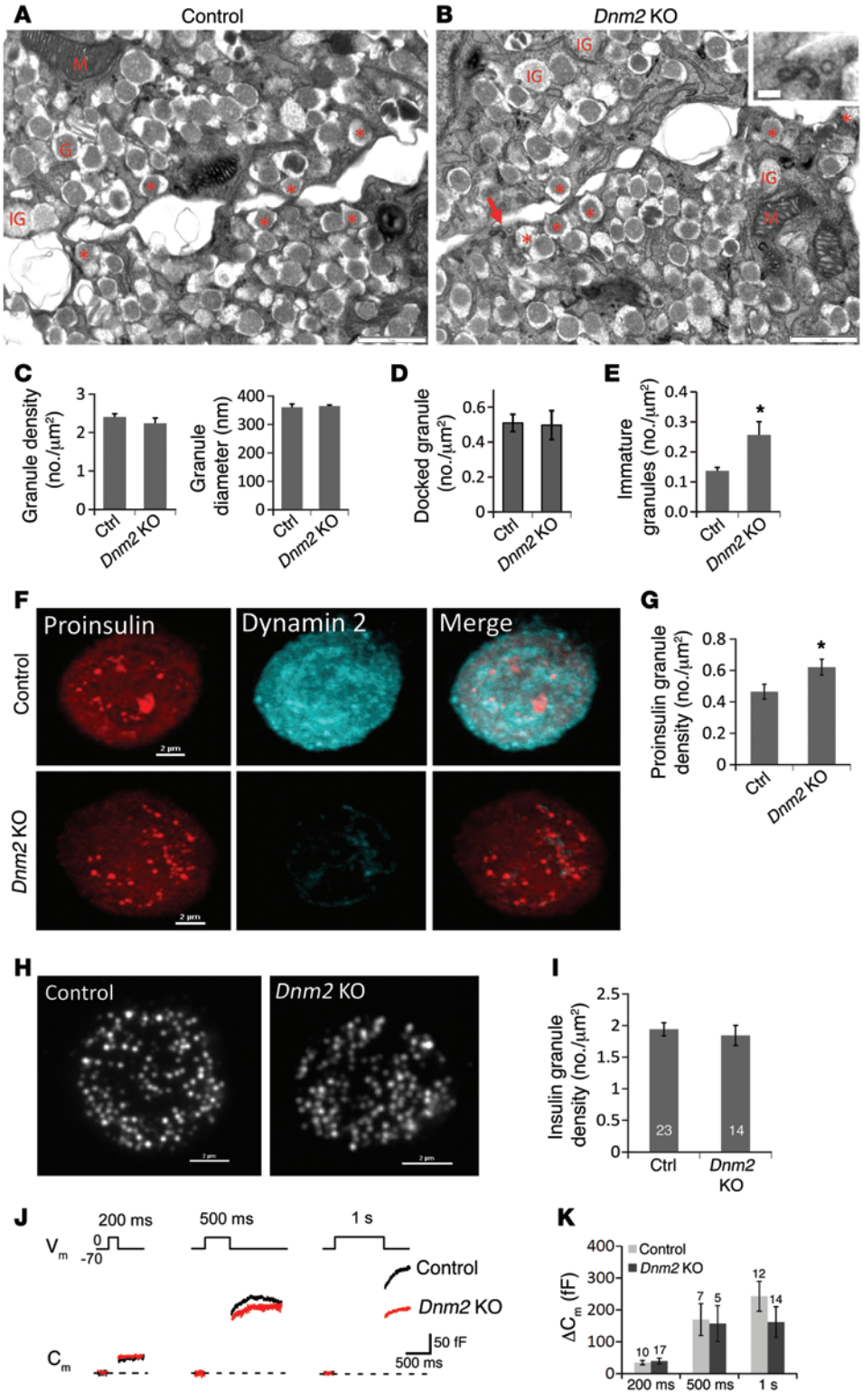

Figure 5. Intact insulin granule biogenesis, docking, and RRP in *Dnm2* KO β cells. (**A** and **B**) EM of a control and *Dnm2* KO β cell. The arrow indicates endocytic intermediates underneath the PM. Note the abundant insulin granules with similar diameter in *Dnm2* KO β cells. Asterisks denote granules docked to the PM. M, mitochondria; G, insulin granule; IG, immature granule. (**C**) Morphological analysis of insulin granule density and size, (**D**) the docked granules, and (**E**) immature granule density (P = 0.017, 2-tailed t test) (n = 8–10 cell sections randomly selected). (**F**) Proinsulin granules visualized in the z-stack projections of confocal images (at a 300 nm z-step). (**G**) Average proinsulin granule density in control (n = 24) and KO (n = 17) β cells (P = 0.0297, 2-tailed t test). (**H**) Insulin granules visualized under TIRFM in a representative control cell and KO β cells. (**I**) Average insulin granule density under TIRFM from control (n = 23) and dynamin 2 KO (n = 14) cells. (**J**) Average C_m traces and (**K**) C_m changes induced by different short depolarizing pulses. The cell numbers in each experiment are shown above the bars (P > 0.05, 2-tailed t test). Scale bars: 1 μm (**A** and **B**); 100 nm (**B**, inset); 2 μm (**F** and **H**). *P < 0.05.

Supplemental Figure 5, B and C), even under 20 mM glucose stimulation for 20 minutes (Supplemental Figure 5D). Moreover, we observed no obvious cell surface expansion in KO cells, which is different from the severe vesicle depletion at nerve terminals after dynamin perturbations (31, 38).

Mature and immature types of insulin granules are readily distinguishable in our preparations based on their characteristic ultrastructures. Typical mature granules contained a dense core with a halo; immature granules were fully filled with homogeneous and much lighter electron density and had tight-fitting membrane (Supplemental Figure 6). These observations were consistent with previous immuno-EM studies (52, 53). The immature granules were more frequently observed in *Dnm2* KO β cells (Supplemental Figure 5B), and their density was slightly

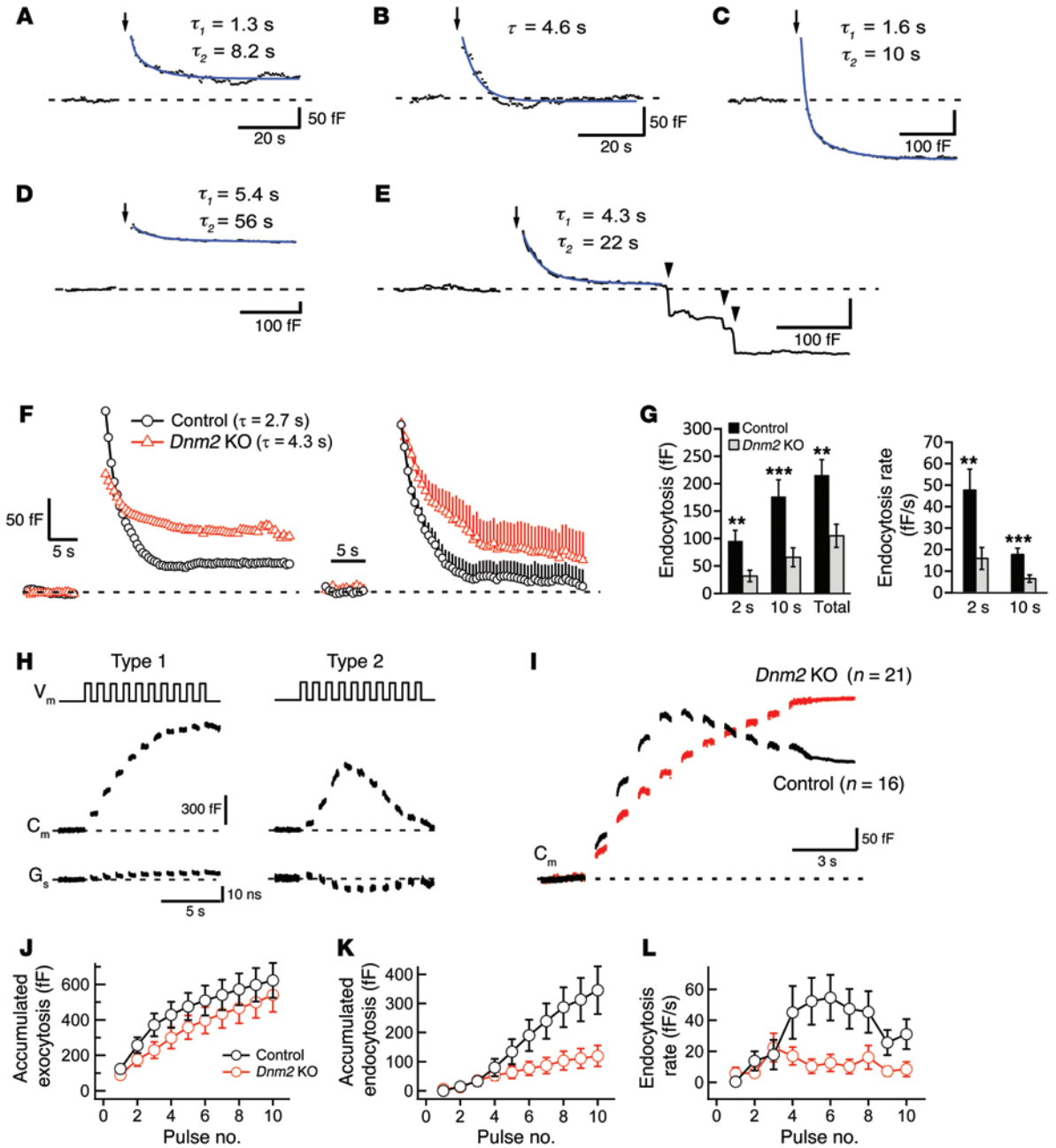

Figure 6. Impaired exocytosis-endocytosis coupling in β cells in the absence of dynamin 2. (**A**–**E**) Real-time C_m recordings showed endocytosis heterogeneity in amplitude and kinetics in different wild-type β cells. Arrows indicate the depolarizing pulse (0 mV, 1-second pulse in **A**–**D**; 0.5-second pulse in **E**); arrowheads in **E** indicate the large, stepwise C_m decreases. (**F**) Average C_m traces triggered by a single depolarization (0 mV, 1 second) from control (n = 15 cells) and *Dnm2* KO cells (n = 14). The time constants of C_m decays are 2.7 seconds and 4.3 seconds for control and KO cells, respectively. The right panel shows the normalized C_m traces. Note the slower C_m decay and incomplete C_m recovery in KO cells. (**G**) The amplitude and speed of C_m decay at 2 seconds ($P < 0.01$) and 10 seconds ($P < 0.005$) after the depolarization (n = 15 and 14 for control and KO, respectively, unpaired 2-tailed t test). (**H**) Exocytosis-dominant (type-1) and endocytosis-dominant (type-2) C_m changes elicited by a train of pulses (ten 500-ms pulses, 0 mV, 1 Hz) in different β cells from wild-type mice. (**I**) The average C_m traces from control (n = 16) and *Dnm2* KO (n = 21) groups. (**J**–**L**) Cumulative exocytosis and endocytosis and endocytosis rate during the train stimulation. $^{**}P < 0.01$, $^{***}P < 0.005$.

higher than that in controls (Figure 5E, $P < 0.05$, 2-tailed t test). Likewise, proinsulin fluorescence imaging revealed a small but significant increase of proinsulin granule density in KO β cells (Figure 5, F and G). These data indicate a potential role of dynamin 2 in insulin granule biogenesis or maturation in β cells, which is in line with the proposed dynamin function in intracellular membrane trafficking in nonsecretory cells (refs. 48, 49, 54, 55 but see also ref. 50). However, the presence of abundant mature granules in dynamin 2 KO β cells does not support an indispensable role of dynamin 2 in insulin granule biogenesis at normal conditions, at least it is not the rate-limiting step in the granule trafficking cycle.

We next estimated the docked insulin granule number by TIRFM that detects granules within approximately 100 nm above the PM. We found no difference in granule density between control and KO β cells (Figure 5, H and I), consistent with the intact granule docking under EM. Moreover, we evaluated the functional RRP size (56) by cell membrane capacitance (C_m) under whole-cell patch-clamp (57) (by single pulse with variable length, Figure 5, J and K). A 200-ms pulse elicited a similar C_m increase in both control (n = 10) and KO β cells (n = 17), respectively ($P > 0.05$); the longer pulses induced larger C_m elevations, but there was no significant difference between control and KO cells (n = 7 and 5 for 0.5 s; n = 12 and 14 for 1 s; $P > 0.05$ for both cases, t test). Therefore, the functional RRP size was not significantly changed in KO β cells (Figure 5, J and K), which is in line with the similar insulin secretion induced by 30 mM KCl (Figure 3, B and E).

Dynamin 2 is critical for efficient exocytosis-endocytosis coupling in pancreatic β cells. The molecular nature of endocytosis is poorly understood in β cells. We directly monitored the membrane retrieval right after insulin exocytosis using capacitance measurements. β Cells were first identified by their relatively larger size compared to other islet cells and the characteristic Na^+ channel inactivation (ref. 57 and Supplemental Figure 7A). Endocytosis in control β cells was largely heterogeneous, both in kinetics and in amplitude from cell to cell (Figure 6, A–E), although it can be fairly consistent in a given cell with the same stimulation (Supplemental Figure 7C). C_m often decayed with single or double exponential kinetics, accompanied occasionally by large downward C_m steps (arrowheads in Figure 6E). Similar properties were observed in *Dnm2* KO β cells, and the average C_m trace still decayed rapidly. However, the decay time constant of the average C_m trace was much slower in KO cells (τ = 4.3 s, n = 14) than in control cells (τ = 2.7 s, n = 15) (Figure 6F). Given the critical role of dynamin 2 in multiple forms of endocytosis in nonneuronal cells (32, 45, 54, 58), it is surprising that the membrane retrieval was not blocked by the depletion of dynamin 2, an abundant dynamin isoform in β cells, indicating the presence of dynamin 2 independent endocytosis in these cells.

To mimic the burst electrical activity in islets, we applied a train of pulses (0 mV, ten 500-ms pulses at 1 Hz) to β cells (Figure 6H, top). Consistent with previous reports (25, 26), we observed largely variable C_m changes during whole-cell C_m recordings. Figure 6H shows two types of typical C_m responses: an exocytosis-dominant C_m response (type-1, which has a continuous C_m increase and subsequent C_m plateau) and an endocytosis-dominant C_m response (type-2, which shows an initial C_m increase followed by a pronounced C_m decrease). The majority of recordings exhibited a mixture of these two types of C_m changes. To avoid potential bias in data classification, we simply pooled the C_m traces together for each genotypes (n = 16 in control; n = 21 in KO) (Figure 6I). The averaged C_m in KO cells displayed a continuous C_m increase (type-1) during train stimulation, which contrasts with the C_m decline following an initial, transient C_m increase (type-2 like) in control cells. The impaired endocytosis in KO cells may explain this difference, since C_m reflects the net change of surface area. Further quantitative analysis by extracting the exocytosis and endocytosis components of C_m data (37) suggested a marked reduction of endocytosis, but not exocytosis, in KO cells (Figure 6, J–L). Thus, dynamin 2 deletion impairs the efficiency of exocytosis and endocytosis coupling in β cells, and dynamin 2 is crucial for the optimal rate of membrane retrieval but is not indispensable.

Impaired CME and abnormal endocytic ultrastructure in β cells in the absence of dynamin 2. Distinct membrane retrieval kinetics in β cells suggests the presence of multiple endocytic pathways. We next used a transferrin uptake assay to evaluate CME in the absence of dynamin 2. Although weak transferrin fluorescence was still visible beneath the PM in *Dnm2* KO β cells, transferrin–Alexa Fluor 568 internalization was significantly reduced (Figure 7, A and B), suggesting the impaired CME in KO cells.

We next characterized β cell endocytosis at ultrastructural levels. Close inspections of EM images revealed that more abundant endocytic intermediates accumulated on the PM in KO β cells than in controls (Figure 7, C–F), and this difference was further enhanced after 20 mM glucose stimulation for 20 minutes (Figure 7F and Supplemental Figure 5D). CCPs in KO β cells tended to have narrower and longer necks than those in controls (Figure 7, C and D), and CCPs were occasionally interconnected with a narrow membrane tubule (Figure 7C, inset) which was unique to *Dnm2* KO cells.

Further EM tomography analysis revealed a striking accumulation of CCPs and unique endocytic intermediate structures in 3 dimensions that were connected to the PM through narrow tubules in *Dnm2* KO cells (Figure 7, G–M). Some CCPs were directly connected to the PM with a single narrow tubule (Figure 7, H and I), and many endocytic intermediates formed more complex structures, in which multiple CCPs interconnected to the same tubule or large vacuoles still connected to cell surface by a narrow tubule (Figure 7, J–M). The meandering tubules in KO β cells were approximately 20 to 80 nm in diameter and up to hundreds of nanometers in length. These structures are reminiscent of endocytic defects in central synapses lacking dynamin 1 (and dynamin 3) (36, 38, 40) but more complicated than those in fibroblasts lacking dynamin (45). A unique feature of these endocytic intermediates is that each tubule was capped by a CCP, suggesting a severe defect in the membrane fission reactions of CME.

Dynamin 2 regulates F-actin organization and insulin granule recruitment to the PM. The pronounced impairment of the second phase of GSIS in *Dnm2* KO mice is strikingly similar to the effect of perturbations in actin regulatory proteins, such as Cdc42 (13), PAK1 (15), RAC1 (14), and N-WASP (16). We therefore examined the actin organization in *Dnm2* KO β cells. Indeed, F-actin fluorescence (Alexa Fluor 488–conjugated phalloidin) was much stronger in KO β cells than in controls, with distinct spatial reorganization (Figure 8, A and B). F-actin filaments in control cells were relatively long and smooth, and they formed a loose and thin meshwork beneath the PM in 3 dimensions (Figure 8C). In contrast, KO β cells showed a strikingly disorganized and thicker F-actin network that was composed of crowded, shorter actin filaments and abundant, dense actin patches/puncta in all dimensions (Figure 8, A and C).

Because the dynamin 2 deletion in β cells is temporally controlled by acute administration of tamoxifen at adulthood, it seems unlikely that the actin reorganization arises from chronic compensation in response to dynamin 2 loss. To further exclude nonspecific effects of *Dnm2* KO, we tested whether reexpression of dynamin 2

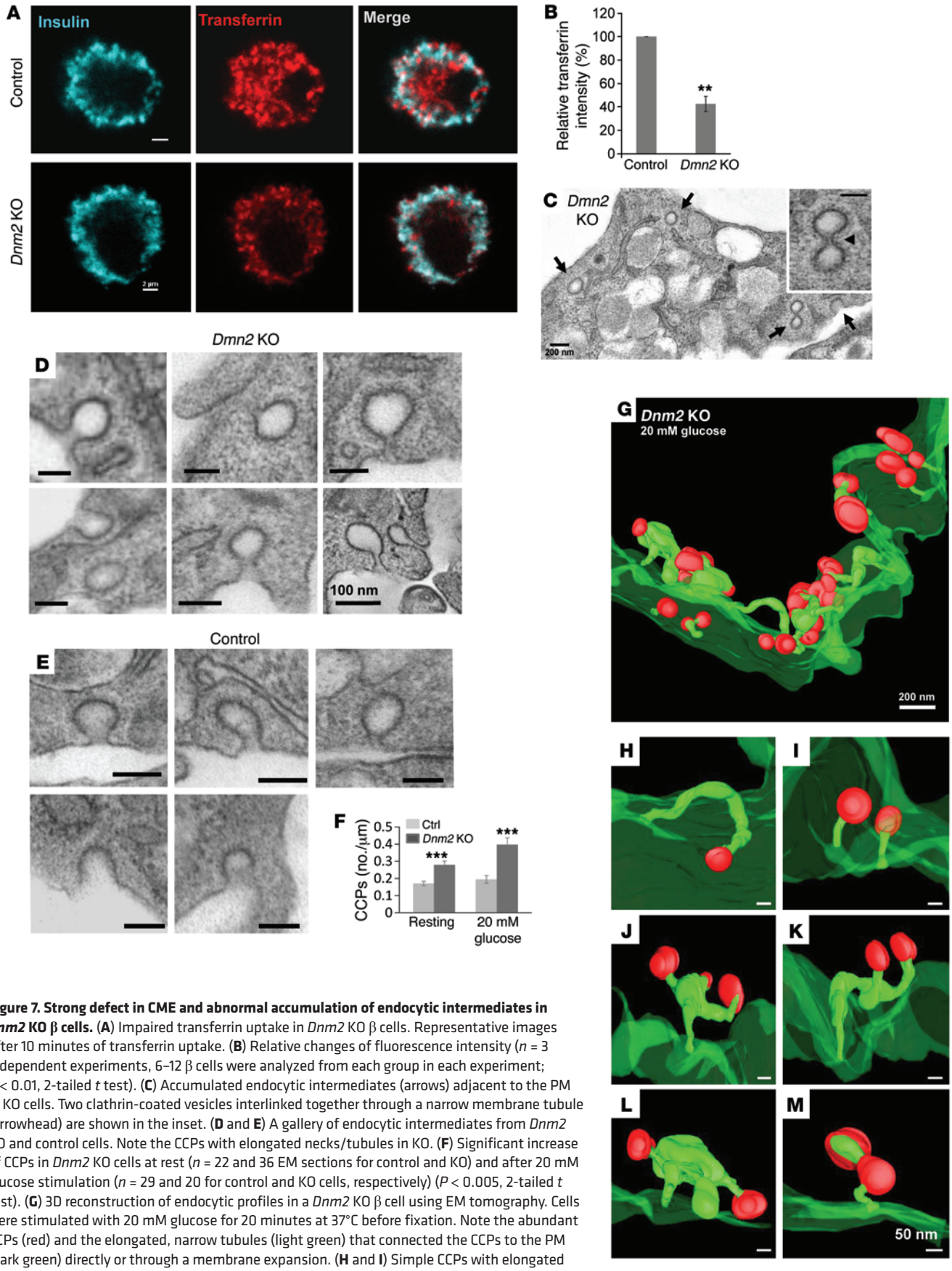

Figure 7. Strong defect in CME and abnormal accumulation of endocytic intermediates in *Dnm2* KO β cells. (**A**) Impaired transferrin uptake in *Dnm2* KO β cells. Representative images after 10 minutes of transferrin uptake. (**B**) Relative changes of fluorescence intensity ($n = 3$ independent experiments, 6–12 β cells were analyzed from each group in each experiment; $P < 0.01$, 2-tailed t test). (**C**) Accumulated endocytic intermediates (arrows) adjacent to the PM in KO cells. Two clathrin-coated vesicles interlinked together through a narrow membrane tubule (arrowhead) are shown in the inset. (**D** and **E**) A gallery of endocytic intermediates from *Dnm2* KO and control cells. Note the CCPs with elongated necks/tubules in KO. (**F**) Significant increase of CCPs in *Dnm2* KO cells at rest ($n = 22$ and 36 EM sections for control and KO) and after 20 mM glucose stimulation ($n = 29$ and 20 for control and KO cells, respectively) ($P < 0.005$, 2-tailed t test). (**G**) 3D reconstruction of endocytic profiles in a *Dnm2* KO β cell using EM tomography. Cells were stimulated with 20 mM glucose for 20 minutes at 37°C before fixation. Note the abundant CCPs (red) and the elongated, narrow tubules (light green) that connected the CCPs to the PM (dark green) directly or through a membrane expansion. (**H** and **I**) Simple CCPs with elongated tubules connected to the cell surface. (**J**–**M**) Complex structures of endocytic intermediates that connected to PM with large, branched membrane vacuoles. Scale bars: 2 μm (**A**); 200 nm (**C** and **G**); 100 nm (**C**, inset, **D**, and **E**); 50 nm (**H**–**M**). $^{**}P < 0.01$, $^{***}P < 0.005$.

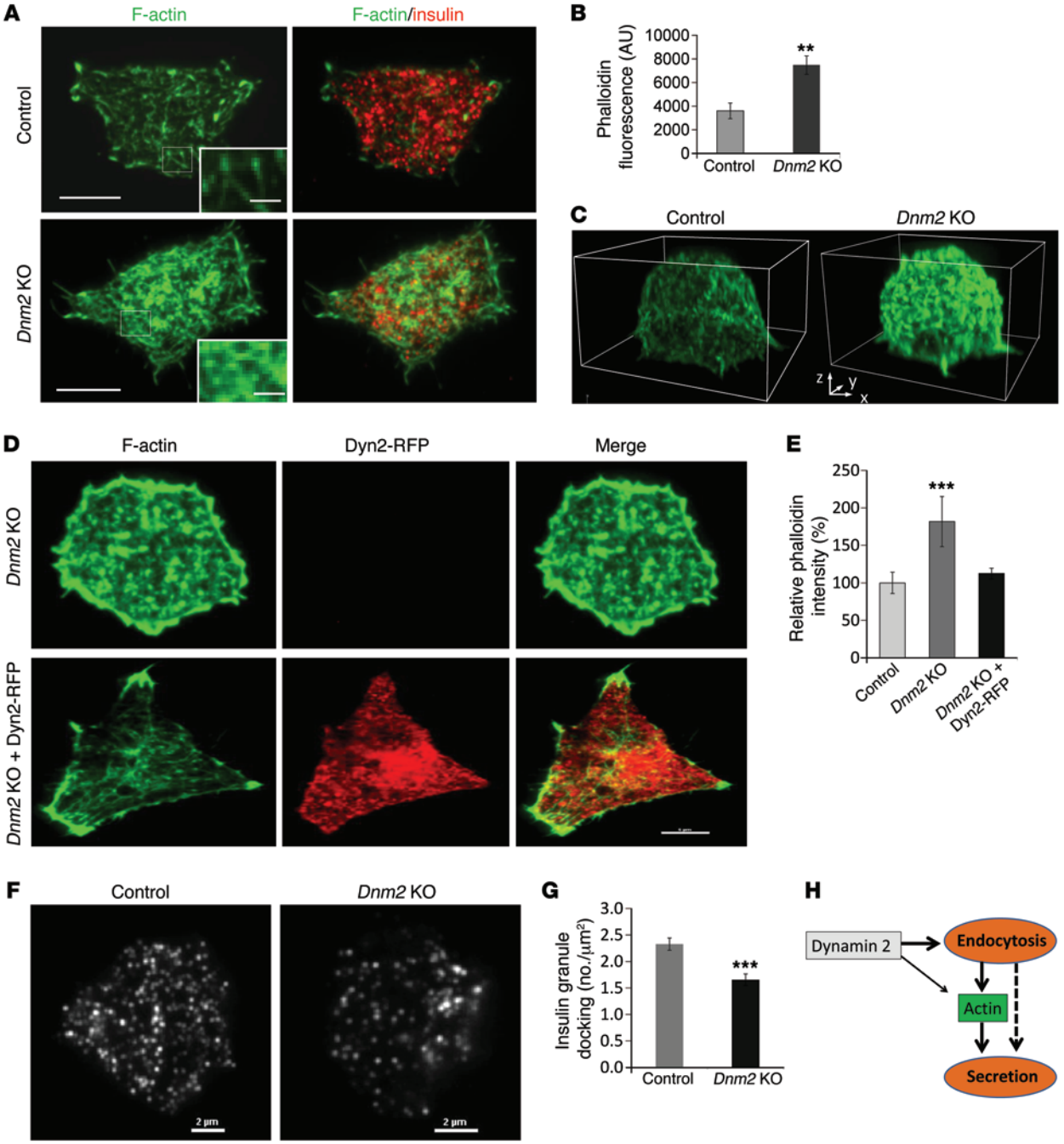

Figure 8. Significant reorganization of F-actin in *Dnm2* KO β cells and impaired insulin granule recruitment to the PM during GSIS. (**A**) TIRFM showing a strong fluorescence increase and structural reorganization of the F-actin network (phalloidin) in a *Dnm2* KO β cell. Insets show the boxed regions at high magnification. (**B**) Average fluorescence intensity of F-actin (n = 10 and 11 cells in control and KO; $P < 0.01$, 2-tailed t test). (**C**) 3D views of the F-actin network under confocal imaging (at 200 nm z-step). (**D**) F-actin changes in *Dnm2* KO β cells were fully rescued by expressing dynamin 2–RFP. (**E**) Relative changes of phalloidin fluorescence intensity in control (n = 36), *Dnm2* KO (n = 15), and *Dnm2* KO cells transfected with dynamin 2–RFP (n = 17 cells; P = 0.002, 1-way ANOVA). (**F**) The number of insulin granules that were recruited to the PM under TIRFM. Cells were equally stimulated with 20 mM glucose and 10 nM GLP-1 for 1 hour at 37°C and fixed immediately. (**G**) Significant decrease in the number of insulin granules recruited to the PM after glucose stimulation (n = 25 and 35 cells for control and KO, respectively; $P < 0.001$, 2-tailed t test). (**H**) The model depicting dynamin regulation of biphasic GSIS through an actin-dependent mechanism in pancreatic β cells. The dashed line denotes other CME-mediated signaling pathways that may also involved. Scale bars: 5 μm (**A** and **D**); 2 μm (**F**); 1 μm (**A**, insets). $^{**}P < 0.01$, $^{***}P < 0.005$.

rescues the abnormal F-actin phenotype in KO β cells. Three days after dynamin 2–red fluorescent protein (dynamin 2–RFP) transfection, KO β cells expressing dynamin 2–RFP fully restored the disorganized F-actin to normal, which contrasted to those cells containing no dynamin 2–RFP in the same cultures (Figure 8, D and E). These data suggest a specific role of dynamin 2 in F-actin reorganization in β cells, consistent with the complex feedback interactions between dynamin and actin during CME (45, 59, 60).

The molecular mechanisms underlying actin regulation of biphasic insulin secretion (10, 61) are poorly understood. One possibility is that the reorganized F-actin inhibits insulin release as a physical barrier by impeding granule access to the PM or decrease RRP size, as proposed in chromaffin cells (62, 63). However, this was not supported by intact docked granules and RRP size in KO cells. The second possibility is that dynamin-induced actin reorganization retards granule recruitment at a later stage of secretion. This is supported by the positive role of actin in vesicle transport (64–67) and the pronounced defect in the second-phase secretion (Figure 3), which largely relies on new granule recruitment to the PM (8, 11). To directly test this idea, we incubated β cells for 1 hour with 20 mM glucose and 10 nM glucagon-like peptide-1 (GLP-1), an incretin peptide that increases insulin secretion through cAMP- and VAMP8-dependent mechanisms (68). Indeed, the treatment revealed a significant decrease of insulin granule density under TIRFM in KO β cells (Figure 8, F and G), suggesting a defect of insulin granule recruitment during GSIS, which is consistent with the proposed actin function in granule replenishment (11, 61).

Given the tight link between dynamin and actin during endocytosis (69) and the critical role of actin in the second phase of GSIS (11, 61), it is conceivable that dynamin 2–dependent endocytosis regulates biphasic insulin release, at least in part, through actin-dependent recruitment of new granules to the PM at the late stage of GSIS (Figure 8H). It will be of special interest to investigate the molecular interactions among dynamin, actin, and insulin granules during GSIS in the future.

Discussion

In this study, we provide the first genetic evidence in vivo to our knowledge that dynamin 2 is required to preserve normal glucose homeostasis and biphasic insulin secretion through endocytosis regulation of granule membrane trafficking. Interestingly, dynamin 2 played a prominent role in the second phase of GSIS, with little effect on insulin granule docking and RRP size. Moreover, dynamin 2 was critical for the efficient coupling of insulin granule exocytosis/endocytosis and the membrane fission reactions at the late stage of CME, but it was not essential for insulin granule biogenesis from the TGN in β cells under basal conditions. Finally, dynamin 2 deletion led to striking F-actin reorganization in KO β cells that can be fully restored by reexpression of dynamin 2. F-actin remodeling contributed to the recruitment of insulin granules to the PM for release during GSIS. Thus, this study revealed a regulatory function of dynamin in biphasic insulin secretion in pancreatic β cells and indicated a potential link between endocytosis and diabetes through the homeostatic control of membrane trafficking.

The molecular nature of endocytic machinery in pancreatic β cells. We found that both dynamin 2 and 3 are coexpressed in mouse pancreatic β cells; this is different from other types of LDCV-secreting cells, such as chromaffin cells (41), PC12 cells (27), HIT-T15 cells, and INS-1 cells (70), in which both dynamin 1 and 2 are expressed. The 3 dynamin isoforms in mammals contain the same domain organization, with 80% identity in encoding DNA sequences, and they independently contribute to membrane endocytosis with largely overlapping function (32). It will be interesting to examine whether dynamin 2 and 3 have differential functions in β cells.

In spite of the vigorous insulin granule recycling in β cells and high levels of dynamin 2 expression, dynamin 2 deletion caused neither granule reduction nor cell surface expansion (Figure 5, A–C, and Figure 4E). Exocytosis-endocytosis coupling was impaired but not blocked in *Dnm2* KO cells, since a substantial amount of endocytosis remained (Figure 6). These results were unexpected. It is unlikely that developmental compensation plays a significant role here, because *Dnm2* was deleted selectively in β cells under temporal control at adulthood. The conditionally targeted gene deletion can also rule out the potential complications of alternative loss-of-function approaches (71), such as off-target effects (of siRNA knockdown, pharmacological inhibitors, ref. 71; and acute photoinactivation, ref. 72) or dominant-negative effects (73) of dynamin mutations. Moreover, the full restoration of normal F-actin organization by dynamin 2 reexpression in KO β cells suggests a specific role of dynamin 2. Thus, dynamin 2 is not essential for β cell endocytosis per se but is critical for an optimal rate of membrane retrieval.

In *Drosophila shibire* mutants (31, 74), endocytosis deficiency is very severe, as demonstrated by a block of endocytosis, vesicle depletion, and extensive cell surface expansion of nerve terminals after stimulation. In comparison, we observed different results in dynamin 2 KO β cells. The simple explanation for this discrepancy is that β cells have access to dynamin 2–independent forms of endocytosis. For example, low levels of dynamin 3 (and possibly extremely low levels of dynamin 1) may, at least partially, support endocytosis in *Dnm2* KO β cells. A similar scenario has been reported at rodent nerve terminals lacking dynamin 1 (36, 75), in which dynamin 3 partially supports vesicle recycling (38, 39). It is unclear whether the dynamin-independent endocytosis at some nonsecretory cells (45, 71) and nerve terminals (i.e., bulk endocytosis) (40, 72, 76) also occurs in dynamin 2 KO β cells. Future study using triple dynamin KO cells will shed new light on this question.

Strongly impaired CME in the absence of dynamin 2 in β cells. Both impaired transferrin uptake and aberrant ultrastructure revealed by EM in *Dnm2* KO β cells demonstrated a crucial function of dynamin 2 in CME. Further, 3D EM tomography revealed that most PM-detached CCPs captured in individual EM sections were actually connected to the PM in KO β cells and represented endocytic intermediates after insulin release, suggesting the impairment of membrane fission at a late stage of CME in the absence of dynamin 2.

The endocytic intermediate structures captured by EM in dynamin 2 KO β cells (Figure 7, G–M) also shed new light on the fate of insulin granules after their full fusion. After insulin granule exocytosis and collapse onto the PM, the granule membrane components may be recaptured selectively as a whole unit or internalized by CME after being broken into smaller pieces. Both scenarios of LDCV membrane retrieval have been proposed in chromaffin cells (77, 78). Abundant accumulation of CCPs indicates the significant role of CME among other forms of endocytosis in β cells. The size of CCPs was approximately 100 nm in diameter, which was only about one-third the size of insulin granules (360 ± 12 nm, $n = 6$ control cells). Thus, membrane components of insulin granules after full fusion most likely split and resort into smaller pieces for CME.

Endocytic control of biphasic GSIS in mouse pancreatic β cells. This study is the first demonstration to our knowledge that dynamin 2–mediated endocytosis regulates plasma glucose homeostasis through changing the insulin secretion capacity of β

cells. It underscores the crucial role of dynamin 2 in biphasic insulin secretion and suggests endocytic control of hormone secretion in vivo. Along the same line, two recent studies provided extra evidence that aberrant endocytic trafficking in β cells may contribute to the pathophysiology of diabetes (79, 80).

The strong decline of insulin secretion in *Dnm2* KO islets was in agreement with the previous work showing the secretion inhibition by overexpression of dynamin K44A or dynamin 2 siRNA knockdown in insulin-secreting cell lines (23). Moreover, interestingly, the decline occurred prominently in the second phase of GSIS. This secretion deficit is unlikely to have resulted from impaired insulin granule biogenesis, because insulin granules in the KO β cells were still abundant in our experiments (Figure 5, A–C). This phenotype apparently differs from that of nerve terminals lacking the dominant dynamin isoform (dynamin 1), in which synaptic vesicle number significantly decreases due to impaired vesicle reformation (36, 75). Thus, the mechanisms underlying dynamin-mediated secretion function between the LDCVs in endocrine cells and the small synaptic vesicles at nerve terminals may be different.

The selective reduction of the second phase of GSIS in *Dnm2* KO mice shows striking parallel with the reduced insulin secretion after perturbations of actin remodeling (13–15, 81), a key factor that selectively contributes to the second phase (10, 11). Accordingly, enhanced actin disassembly by PPARβ/δ (17) or the actin-capping protein gelsolin (81) increases the second phase. In *Dnm2* KO β cells, F-actin was largely reorganized at the cortical layer (Figure 8, A–C), and this change can be fully rescued by reintroducing dynamin 2 into these cells (Figure 8, D and E), suggesting a specific causal relationship between dynamin 2 and actin reorganization in β cells. These data support a specific role of dynamin 2–mediated actin remodeling in the regulation of GSIS in β cells and highlight its potential relevance to the pathogenesis of T2D. In support of this idea, human islets of patients with T2D exhibit a strong decrease (80% less than controls) in P21-activated kinase PAK1, a downstream effector of Cdc42 and RAC1 signaling that controls cytoskeletal remodeling. Furthermore, PAK1 inhibition in nondiabetic islets leads to a selective reduction of the second phase of GSIS (15). Finally, diabetic islets from humans with T2D (82) contained ~10 times higher levels of total actin than controls, and a similar higher level of actin has also been reported in Goto-Kakizaki rats (83, 84).

Multiple roles of actin have been increasingly discovered to regulate membrane trafficking (85), but its exact molecular function remains poorly understood. Both a negative role as a physical fusion barrier and a positive role of promoting vesicle transport and exocytosis have been proposed (86, 87). In insulin-secreting cells, a fairly selective role of actin remodeling in the second phase of GSIS has been reported (11, 13, 14, 16, 61). Similarly, we observed a selective decrease in the second phase of GSIS along with strong actin reorganization in *Dnm2* KO β cells. Our morphological and functional data suggest that insulin granule docking and RRP size were normal at rest in *Dnm2* KO cells (Figure 5); this is consistent with the minor difference between control and KO islets in initial release induced by both glucose (the first phase) and direct depolarization (30 mM KCl or short depolarization). Therefore, the F-actin reorganization in KO β cells does not differentially affect RRP granules compared with control cells (Figure 3). On the other hand, TIRFM demonstrated a significant decrease in fusion events during the second phase (Figure 3), with a significant decrease in the number of insulin granules beneath the PM at the later stage of GSIS in KO cells (Figure 8, F and G). These data demonstrated a defect in insulin granule recruitment from the reserve pool to the PM in *Dnm2* KO β cells after the RRP granules run out, providing a direct cellular explanation for the selective decline of the second phase of GSIS in KO mice.

Dynamin may regulate actin function through both direct and indirect mechanisms in β cells. First, dynamin interacts with actin cytoskeleton through direct binding to F-actin (88) and microtubules (89) or through indirect interactions with actin-binding/regulatory molecules (90–92). For example, dynamin can directly bind actin filaments through a conserved actin-binding domain between amino acid 399 and 444, and the point mutation of this domain specifically decreases the dynamin-binding affinity to actin without affecting endocytosis (88). Dynamin self-oligomerization after actin binding promotes the elongation of short F-actin by removing the actin-capping protein gelsolin from the barbed end of actin filaments. The shorter disorganized F-actin observed in dynamin 2 KO β cells is in line with a defect of dynamin-dependent actin elongation. Second, dynamin regulates actin reorganization through a mechanism downstream of the CME, where the complex actin-dynamin interactions occur (45, 59, 60, 69). For instance, clathrin coats arrested on the PM are required for nucleating the actin regulators and polymerizing actin at CCPs (45). Third, some CME-mediated signaling pathways may also contribute to the actin remodeling. In fibroblasts lacking dynamin, the activated Cdc42-associated kinase (Ack) is activated and concentrated at clathrin-coated pits through direct binding to clathrin heavy chain (93).

Figure 8H depicts a model based on the above data. During insulin granule trafficking, dynamin 2 regulates endocytosis as the major membrane fission machinery, particularly in CME. Clathrin and dynamin 2 on CCPs orchestrate actin function through direct and/or indirect molecular interactions to optimize its role in typical biphasic GSIS. In *Dnm2* KO β cells, accumulation of the arrested CCPs on the PM due to fission defects impairs normal F-actin network, and this actin disorganization further causes a defect in granule recruitment to the PM that is critical for the second phase of GSIS. This model explains the impaired biphasic GSIS and glucose intolerance in *Dnm2* KO mice. However, it is important to note that dynamin 2–mediated endocytosis controls the abundance and turnover of cell surface molecules, some of which may also be involved in GSIS through different signaling pathways (Figure 8H, dashed line).

In summary, using temporally controlled and β cell–specific gene ablation, we have provided compelling evidence both in vivo and in vitro that dynamin 2 is required for normal glucose homeostasis through direct regulation of biphasic insulin secretion from pancreatic β cells. Depletion of dynamin 2 caused a severe CME defect and subsequent aberrant actin reorganization; impaired granule recruitment from the reserve pool to the PM contributed to the prominent decline of the second phase of GSIS in *Dnm2* KO mice (Figure 8H). This study has uncovered a pivotal role of dynamin 2–mediated endocytosis in regulating pancreatic β cell secretory function by orchestrating membrane trafficking homeostasis and F-actin remodeling, indicating a potential link between endocytosis and the pathophysiology of diabetes.

Methods

Generation of temporally controlled, β cell–specific Dnm2 KO mice. Mice carrying floxed sites in the exon 2 of dynamin 2 gene (*Dnm2*$^{fl/fl}$ mice) (45) were crossed with *Tg(Ins1-cre/ERT)1Lpi* (also termed *MIP1-CreERT*) transgenic mice (46). *Dnm2*$^{fl/fl}$ mice were provided by Pietro De Camilli (Yale University, New Haven, Connecticut, USA). Mouse genotypes were determined by PCR. *Dnm2*$^{fl/fl}$*MIP1-CreER* mice and age-matched littermate controls (*Dnm2*$^{fl/fl}$) were paired for experiments whenever possible; age-matched black-6 mice were occasionally used in some earlier experiments. Mice were administrated at an age of 1 to 3 months with tamoxifen (47) (0.15 g/kg body weight dissolved in corn oil as vehicle, injected i.p., once a day) for 10 days, and experiments started approximately 4 weeks after the first treatment. Approximately 76% to 94.3% of β cells showed efficient dynamin 2 depletion, depending on the experimental conditions.

Glucose tolerance tests and insulin tolerance tests. For glucose tolerance tests (GTTs), blood was sampled from mouse tail veins at 0, 15, 30, 60, and 120 minutes after glucose injection (i.p., 2 g/kg body weight) in the fasted mice (for 14 hours), and glucose levels were measured by glucose meters (OneTouch-Ultra2, LifeScan Inc., or TRUEresult, Nipro Diagnostics Inc.). For insulin tolerance tests (ITTs), mice fasted for approximately 6 hours were i.p. injected with Novolin R (0.75 units/kg body weight; Novo Nordisk Inc.) before blood sampling. Age-matched littermates (*Dnm2*$^{fl/fl}$*MIP1-CreERT* and *Dnm2*$^{fl/fl}$ mice after injections of vehicle with and without tamoxifen) were used for GTTs to minimize the variation in gene background, intrauterine environment, etc. For high-fat diet experiments, mice were fed with high-fat diet (D12331, 58 kcal% fat with sucrose, Research Diets Inc.) for 3 months before experiments (for details, see the Supplemental Methods).

Pancreatic islet isolation and β cell cultures. Pancreatic islets of Langerhans and individual islet cells were isolated and cultured as previously described (57) with minor modifications (see the Supplemental Methods).

Islet perifusion, insulin secretion assays, and Western blotting. Islet perifusion was performed at 37°C using a system designed in-house. Isolated islets of equal number (between 30 and 50) and size were paired between control and KO mice in each experiment. Islets were perifused with Krebs-Ringer bicarbonate buffer (KRBB); fractions collected in 96-well plates were used for insulin tests with insulin AlphaLISA (94). Purified islets were homogenized in lysis buffer for Western blotting (see the Supplemental Methods for details).

Patch-clamp and C_m measurements. β Cells grown on coverslips were patch clamped at 34°C to 36°C, and whole-cell capacitance measurements were performed as previously described (37, 57) (see the Supplemental Methods for details).

Immunofluorescence staining. Pancreata were fixed with 4% paraformaldehyde (PFA) plus 4% sucrose in 0.12 M sodium phosphate buffer, embedded in OCT, and cut in 8-μM frozen sections. Cells grown on coverslips were fixed with 2% PFA. Samples were first processed for immunostaining with the primary antibodies and then with fluorescence-conjugated secondary antibodies (see the Supplemental Methods).

Spinning disk confocal and TIRF imaging. Fluorescence imaging was performed with the confocal and TIRF imaging system based on a Nikon Ti-E Eclipse inverted microscope (see the Supplemental Methods). Imaging 3D reconstruction, fluorescence analysis, and quantification were done using NIS-Elements (Nikon). Images for comparisons were acquired and displayed in the same settings for both control and *Dnm2* KO cells unless specified. The insulin granules under TIRF were define as docked granules and counted using NIS spot detection function. For Figure 8F, cells preincubated with 10 nM GLP-1 for 30 minutes were stimulated with 20 mM glucose and 10 nM GLP-1 for 1 hour at 37°C and fixed immediately. For F-actin rescue experiments, β cell cultures were transfected with dynamin 2–RFP (provided by Pietro De Camilli) using Lipofectamine 2000 and fixed after 3 days of expression.

Live-cell TIRF imaging of insulin granule fusion. NPY-pHluorin was generated by replacing EGFP in NPY-EGFP plasmid with the pH-sensitive pHluorin (both NPY-EGFP and pHluorin were provided by Pietro De Camilli). NPY-pHluorin has the advantage of a higher signal/noise ratio for fusion events due to its pH sensitivity, and it is more sensitive to granule fusion events than NPY-EGFP, although it provides no information on granule dynamics before fusion. β Cells were transfected with NPY-pHluorin with Lipofectamine 2000 (Life Technology) and used within approximately 40 hours. Cells were TIRF imaged at 5 Hz (200-ms exposure), with 2 × 2 pixel binning at 35°C to 37°C, and the continuous perfusion of KRBB or 20 mM glucose in KRBB (pH = 7.3) was applied. All fusion events detected between 0 and 6 minutes and 7 and 20 minutes during 20 mM glucose perfusion were defined as the first and the second phase, respectively, and were normalized to the individual cell footprint areas (for details, see the Supplemental Methods).

Transferrin uptake assay. Cultured β cells were incubated with Alexa Fluor 568–conjugated transferrin (25 μg/ml, Invitrogen, T23365) in normal culture medium for 10 minutes (37°C) after preincubation in serum-free DMEM for an hour and then washed with acidic buffer and fixed with 2% PFA and imaged later (See the Supplemental Methods).

Cytosolic Ca^{2+} and NADPH imaging. $[Ca^{2+}]_i$ was measured by fura-2 ratiometric fluorescence imaging as described previously (39, 95). NADPH fluorescence imaging was carried out with the same system as the Ca^{2+} imaging (see the Supplemental Methods for details).

EM and EM tomography. EM was carried out as described previously (37), with minor modifications. Purified pancreatic islets were fixed with 2.5% glutaraldehyde in 0.1 M sodium cacodylate buffer for 2 hours and post-fixed in 1% OsO_4, 1.5% $K_4Fe(CN)_6$, and 0.1 M sodium cacodylate for 1 hour. Islets were en bloc stained, dehydrated, embedded, and cut into ultrathin sections (70–90 nm), followed by imaging and analysis (see the Supplemental Methods for details).

For electron tomography, tissue sections (200–250 nm) were imaged in a TECNAI TF20 transmission electron microscope (FEI) operated at 200 kV (Yale Center for Cellular and Molecular Imaging, Yale University) as described previously (40). Contours of membranes were traced using IMOD software manually.

Statistics. All values are presented as mean ± SEM unless otherwise indicated. Statistical analysis was performed using 2-tailed Student's *t* test for 2 groups. One-way ANOVA with post-hoc Tukey honest significant difference test was used to analyze the differences among 3 or more samples. *P* values of less than 0.05 were considered statistically significant.

Study approval. All procedures involving animals were approved by the Institutional Animal Care and Use Committee of the University of Wisconsin-Madison and followed the *NIH Guide for the Care and Use of Laboratory Animals* (8th ed. The National Academies Press. 2011.).

Acknowledgments

This work was supported by NIH grants R01DK093953 (to X. Lou) and P30 NS069271 and Diabetes and Endocrinology Research Center award A07059 (to X. Lou). C. Ji is partially

supported by an American Heart Association predoctoral fellowship (14PRE20380168), Y. Wu is partially supported by NIH R37NS036251, and L.H. Philipson and N. Tamarina are partially supported by NIH grant P30 DK20595. We specially thank Pietro De Camilli for the *Dnm2*$^{fl/fl}$ mice, for discussion, and for the generous support of the Pietro De Camilli lab in some experiments. We thank Laura Funk, Heather Czapla, and Satyajit Mahapatra for technical support and discussion and Meyer Jackson, Ed Chapman, Tim Gomez, and Alan Attie for reading the manuscript and for their suggestions.

Address correspondence to: Xuelin Lou, University of Wisconsin-Madison, Department of Neuroscience, 1111 Highland Avenue, Wisconsin Institutes for Medical Research, Tower 2, Madison, Wisconsin 53705-2275, USA. Phone: 608.263.6265; E-mail: xlou3@wisc.edu.

1. Haucke V, Neher E, Sigrist SJ. Protein scaffolds in the coupling of synaptic exocytosis and endocytosis. *Nat Rev Neurosci*. 2011;12(3):127–138.
2. Saheki Y, De Camilli P. Synaptic vesicle endocytosis. *Cold Spring Harb Perspect Biol*. 2012;4(9):a005645.
3. Ashcroft FM, Rorsman P. Diabetes mellitus and the beta cell: the last ten years. *Cell*. 2012;148(6):1160–1171.
4. Cerasi E. Mechanisms of glucose stimulated insulin secretion in health and in diabetes: some re-evaluations and proposals. *Diabetologia*. 1975;11(1):1–13.
5. Curry DL, Bennett LL, Grodsky GM. Dynamics of insulin secretion by the perfused rat pancreas. *Endocrinology*. 1968;83(3):572–584.
6. Nunemaker CS, Wasserman DH, McGuinness OP, Sweet IR, Teague JC, Satin LS. Insulin secretion in the conscious mouse is biphasic and pulsatile. *Am J Physiol Endocrinol Metab*. 2006;290(3):E523–E529.
7. Hosker JP, Rudenski AS, Burnett MA, Matthews DR, Turner RC. Similar reduction of first- and second-phase B-cell responses at three different glucose levels in type II diabetes and the effect of gliclazide therapy. *Metabolism*. 1989;38(8):767–772.
8. Rorsman P, Renstrom E. Insulin granule dynamics in pancreatic beta cells. *Diabetologia*. 2003;46(8):1029–1045.
9. Henquin JC, Ishiyama N, Nenquin M, Ravier MA, Jonas JC. Signals and pools underlying biphasic insulin secretion. *Diabetes*. 2002;51(supp 1):S60–S67.
10. Wang Z, Thurmond DC. Mechanisms of biphasic insulin-granule exocytosis - roles of the cytoskeleton, small GTPases and SNARE proteins. *J Cell Sci*. 2009;122(pt 7):893–903.
11. Seino S, Shibasaki T, Minami K. Dynamics of insulin secretion and the clinical implications for obesity and diabetes. *J Clin Invest*. 2011;121(6):2118–2125.
12. Shibasaki T, et al. Essential role of Epac2/Rap1 signaling in regulation of insulin granule dynamics by cAMP. *Proc Natl Acad Sci U S A*. 2007;104(49):19333–19338.
13. Wang ZX, Oh EJ, Thurmond DC. Glucose-stimulated Cdc42 signaling is essential for the second phase of insulin secretion. *J Biol Chem*. 2007;282(13):9536–9546.
14. Wang Z, Thurmond DC. Differential phosphorylation of RhoGDI mediates the distinct cycling of Cdc42 and Rac1 to regulate second-phase insulin secretion. *J Biol Chem*. 2010;285(9):6186–6197.
15. Wang Z, Oh E, Clapp DW, Chernoff J, Thurmond DC. Inhibition or ablation of p21-activated kinase (PAK1) disrupts glucose homeostatic mechanisms in vivo. *J Biol Chem*. 2011;286(48):41359–41367.
16. Uenishi E, et al. Actin dynamics regulated by the balance of neuronal Wiskott-Aldrich syndrome protein (N-WASP) and cofilin activities determines the biphasic response of glucose-induced insulin secretion. *J Biol Chem*. 2013;288(36):25851–25864.
17. Iglesias J, et al. PPARβ/δ affects pancreatic β cell mass and insulin secretion in mice. *J Clin Invest*. 2012;122(11):4105–4117.
18. Boyd AE. Microtubules and β cell function: effect of colchicine on microtubules and insulin secretion in vitro by mouse β cells. *J Cell Biol*. 1982;92(2):425–434.
19. Cui J, et al. Targeted inactivation of kinesin-1 in pancreatic β-cells in vivo leads to insulin secretory deficiency. *Diabetes*. 2011;60(1):320–330.
20. Gaisano HY. Here come the newcomer granules, better late than never. *Trends Endocrinol Metab*. 2014;25(8):381–388.
21. Orci L, Malaisse-Lagae F, Ravazzola M, Amherdt M, Renold AE. Exocytosis-endocytosis coupling in the pancreatic β cell. *Science*. 1973;181(4099):561–562.
22. MacDonald PE, Braun M, Galvanovskis J, Rorsman P. Release of small transmitters through kiss-and-run fusion pores in rat pancreatic β cells. *Cell Metab*. 2006;4(4):283–290.
23. Min L, et al. Dynamin is functionally coupled to insulin granule exocytosis. *J Biol Chem*. 2007;282(46):33530–33536.
24. Tsuboi T, McMahon HT, Rutter GA. Mechanisms of dense core vesicle recapture following "kiss and run" ("cavicapture") exocytosis in insulin-secreting cells. *J Biol Chem*. 2004;279(45):47115–47124.
25. Eliasson L, et al. Endocytosis of secretory granules in mouse pancreatic β-cells evoked by transient elevation of cytosolic calcium. *J Physiol*. 1996;493(pt 3):755–767.
26. He Z, et al. Ca^{2+} triggers a novel clathrin-independent but actin-dependent fast endocytosis in pancreatic β cells. *Traffic*. 2008;9(6):910–923.
27. Hoy M, et al. Inositol hexakisphosphate promotes dynamin I- mediated endocytosis. *Proc Natl Acad Sci U S A*. 2002;99(10):6773–6777.
28. Zhao Y, Fang Q, Straub SG, Lindau M, Sharp GW. Hormonal inhibition of endocytosis: novel roles for noradrenaline and G protein G(z). *J Physiol*. 2010;588(pt 18):3499–3509.
29. Shpetner HS, Vallee RB. Identification of dynamin, a novel mechanochemical enzyme that mediates interactions between microtubules. *Cell*. 1989;59(3):421–432.
30. van der Bliek AM, Meyerowitz EM. Dynamin-like protein encoded by the Drosophila shibire gene associated with vesicular traffic. *Nature*. 1991;351(6325):411–414.
31. Koenig JH, Ikeda K. Disappearance and reformation of synaptic vesicle membrane upon transmitter release observed under reversible blockage of membrane retrieval. *J Neurosci*. 1989;9(11):3844–3860.
32. Ferguson SM, De Camilli P. Dynamin, a membrane-remodelling GTPase. *Nat Rev Mol Cell Biol*. 2012;13(2):75–88.
33. Schmid SL, Frolov VA. Dynamin: functional design of a membrane fission catalyst. *Annu Rev Cell Dev Biol*. 2011;27:79–105.
34. Koenig JH, Yamaoka K, Ikeda K. Omega images at the active zone may be endocytotic rather than exocytotic: implications for the vesicle hypothesis of transmitter release. *Proc Natl Acad Sci U S A*. 1998;95(21):12677–12682.
35. Cao H, Garcia F, McNiven MA. Differential distribution of dynamin isoforms in mammalian cells. *Mol Biol Cell*. 1998;9(9):2595–2609.
36. Ferguson SM, et al. A selective activity-dependent requirement for dynamin 1 in synaptic vesicle endocytosis. *Science*. 2007;316(5824):570–574.
37. Lou X, Paradise S, Ferguson SM, De Camilli P. Selective saturation of slow endocytosis at a giant glutamatergic central synapse lacking dynamin 1. *Proc Natl Acad Sci U S A*. 2008;105(45):17555–17560.
38. Raimondi A, et al. Overlapping role of dynamin isoforms in synaptic vesicle endocytosis. *Neuron*. 2011;70(6):1100–1114.
39. Lou X, et al. Reduced release probability prevents vesicle depletion and transmission failure at dynamin mutant synapses. *Proc Natl Acad Sci U S A*. 2012;109(8):E515–E523.
40. Wu Y, et al. A dynamin 1-, dynamin 3- and clathrin-independent pathway of synaptic vesicle recycling mediated by bulk endocytosis. *Elife*. 2014;3:e01621.
41. Artalejo CR, Elhamdani A, Palfrey HC. Sustained stimulation shifts the mechanism of endocytosis from dynamin-1-dependent rapid endocytosis to clathrin- and dynamin-2-mediated slow endocytosis in chromaffin cells. *Proc Natl Acad Sci U S A*. 2002;99(9):6358–6363.
42. Willinger T, Ferguson SM, Pereira JP, De Camilli P, Flavell RA. Dynamin 2-dependent endocytosis is required for sustained S1PR1 signaling. *J Exp Med*. 2014;211(4):685–700.
43. Lee MY, et al. Dynamin 2 regulation of integrin endocytosis, but not VEGF signaling, is crucial for developmental angiogenesis. *Development*. 2014;141(7):1465–1472.
44. Shin NY, et al. Dynamin and endocytosis are required for the fusion of osteoclasts and myoblasts. *J Cell Biol*. 2014;207(1):73–89.

45. Ferguson SM, et al. Coordinated actions of actin and BAR proteins upstream of dynamin at endocytic clathrin-coated pits. *Dev Cell*. 2009;17(6):811–822.
46. Tamarina NA1, Roe MW, Philipson L. Characterization of mice expressing Ins1 gene promoter driven CreERT recombinase for conditional gene deletion in pancreatic β-cells. *Islets*. 2014;6(1):e27685.
47. Wicksteed B, et al. Conditional gene targeting in mouse pancreatic ss-Cells: analysis of ectopic Cre transgene expression in the brain. *Diabetes*. 2010;59(12):3090–3098.
48. Jones SM, Howell KE, Henley JR, Cao H, McNiven MA. Role of dynamin in the formation of transport vesicles from the trans-Golgi network. *Science*. 1998;279(5350):573–577.
49. Kreitzer G, Marmorstein A, Okamoto P, Vallee R, Rodriguez-Boulan E. Kinesin and dynamin are required for post-Golgi transport of a plasma-membrane protein. *Nat Cell Biol*. 2000;2(2):125–127.
50. Bonazzi M, et al. CtBP3/BARS drives membrane fission in dynamin-independent transport pathways. *Nat Cell Biol*. 2005;7(6):570–580.
51. Liu YW, Lukiyanchuk V, Schmid SL. Common membrane trafficking defects of disease-associated dynamin 2 mutations. *Traffic*. 2011;12(11):1620–1633.
52. Orci L, Ravazzola M, Storch MJ, Anderson RG, Vassalli JD, Perrelet A. Proteolytic maturation of insulin is a post-Golgi event which occurs in acidifying clathrin-coated secretory vesicles. *Cell*. 1987;49(6):865–868.
53. Zhu X, Orci L, Carroll R, Norrbom C, Ravazzola M, Steiner DF. Severe block in processing of proinsulin to insulin accompanied by elevation of des-64,65 proinsulin intermediates in islets of mice lacking prohormone convertase 1/3. *Proc Natl Acad Sci U S A*. 2002;99(16):10299–10304.
54. Liu YW, Surka MC, Schroeter T, Lukiyanchuk V, Schmid SL. Isoform and splice-variant specific functions of dynamin-2 revealed by analysis of conditional knock-out cells. *Mol Biol Cell*. 2008;19(12):5347–5359.
55. Cao H, et al. Actin and Arf1-dependent recruitment of a cortactin-dynamin complex to the Golgi regulates post-Golgi transport. *Nat Cell Biol*. 2005;7(5):483–492.
56. Gillis KD, Mossner R, Neher E. Protein kinase C enhances exocytosis from chromaffin cells by increasing the size of the readily releasable pool of secretory granules. *Neuron*. 1996;16(6):1209–1220.
57. Lou XL, et al. Na^+ channel inactivation: a comparative study between pancreatic islet β-cells and adrenal chromaffin cells in rat. *J Physiol*. 2003;548(pt 1):191–202.
58. Cao H, Chen J, Awoniyi M, Henley JR, McNiven MA. Dynamin 2 mediates fluid-phase micropinocytosis in epithelial cells. *J Cell Sci*. 2007; 120(pt 23):4167–4177.
59. Taylor MJ, Lampe M, Merrifield CJ. A feedback loop between dynamin and actin recruitment during clathrin-mediated endocytosis. *PLoS Biol*. 2012;10(4):e1001302.
60. Grassart A, et al. Actin and dynamin2 dynamics and interplay during clathrin-mediated endocytosis. *J Cell Biol*. 2014;205(5):721–735.
61. Kalwat MA, Thurmond DC. Signaling mechanisms of glucose-induced F-actin remodeling in pancreatic islet β cells. *Exp Mol Med*. 2013;45:e37.
62. Vitale ML, Seward EP, Trifaro JM. Chromaffin cell cortical actin network dynamics control the size of the release-ready vesicle pool and the initial rate of exocytosis. *Neuron*. 1995;14(2):353–363.
63. Nakata T, Hirokawa N. Organization of cortical cytoskeleton of cultured chromaffin cells and involvement in secretion as revealed by quick-freeze, deep-etching, and double-label immunoelectron microscopy. *J Neurosci*. 1992;12(6):2186–2197.
64. Lang T, et al. Role of actin cortex in the subplasmalemmal transport of secretory granules in PC-12 cells. *Biophys J*. 2000;78(6):2863–2877.
65. Schuh M. An actin-dependent mechanism for long-range vesicle transport. *Nat Cell Biol*. 2011;13(12):1431–1436.
66. Yuan T, Lu J, Zhang J, Zhang Y, Chen L. Spatiotemporal detection and analysis of exocytosis reveal fusion "hotspots" organized by the cytoskeleton in endocrine cells. *Biophys J*. 2015;108(2):251–260.
67. Lopez JP, Turner JR, Philipson LH. Glucose-induced ERM protein activation and translocation regulates insulin secretion. *Am J Physiol Endocrinol Metab*. 2010;299(5):E772–E785.
68. Zhu D, et al. Dual role of VAMP8 in regulating insulin exocytosis and islet beta cell growth. *Cell Metab*. 2012;16(2):238–249.
69. Mooren OL, Galletta BJ, Cooper JA. Roles for actin assembly in endocytosis. *Annu Rev Biochem*. 2012;81:661–686.
70. Lu J, He Z, Fan J, Xu P, Chen L. Overlapping functions of different dynamin isoforms in clathrin-dependent and -independent endocytosis in pancreatic β cells. *Biochem Biophys Res Commun*. 2008;371(2):315–319.
71. Park RJ, Shen H, Liu L, Liu X, Ferguson SM, De Camilli P. Dynamin triple knockout cells reveal off target effects of commonly used dynamin inhibitors. *J Cell Sci*. 2013;126(pt 22):5305–5312.
72. Kasprowicz J, Kuenen S, Swerts J, Miskiewicz K, Verstreken P. Dynamin photoinactivation blocks Clathrin and α-adaptin recruitment and induces bulk membrane retrieval. *J Cell Biol*. 2014;204(7):1141–1156.
73. Doyon JB, et al. Rapid and efficient clathrin-mediated endocytosis revealed in genome-edited mammalian cells. *Nat Cell Biol*. 2011;13(3):331–337.
74. Kosaka T, Ikeda K. Reversible blockage of membrane retrieval and endocytosis in the garland cell of the temperature-sensitive mutant of Drosophila melanogaster, shibirets1. *J Cell Biol*. 1983;97(2):499–507.
75. Lou X, Paradise S, Ferguson SM, De Camilli P. Selective saturation of slow endocytosis at a giant glutamatergic central synapse lacking dynamin 1. *Proc Natl Acad Sci U S A*. 2008;105(45):17555–17560.
76. Xu J, McNeil B, Wu W, Nees D, Bai L, Wu LG. GTP-independent rapid and slow endocytosis at a central synapse. *Nat Neurosci*. 2008;11(1):45–53.
77. Bittner MA, Aikman RL, Holz RW. A nibbling mechanism for clathrin-mediated retrieval of secretory granule membrane after exocytosis. *J Biol Chem*. 2013;288(13):9177–9188.
78. Ceridono M, et al. Selective recapture of secretory granule components after full collapse exocytosis in neuroendocrine chromaffin cells. *Traffic*. 2011;12(1):72–88.
79. Deisl C, et al. Sodium/hydrogen exchanger NHA2 is critical for insulin secretion in β-cells. *Proc Natl Acad Sci U S A*. 2013;110(24):10004–10009.
80. Wen D, et al. Bulk-like endocytosis plays an important role in the recycling of insulin granules in pancreatic β cells. *Protein Cell*. 2012;3(8):618–626.
81. Tomas A, Yermen B, Min L, Pessin JE, Halban PA. Regulation of pancreatic β-cell insulin secretion by actin cytoskeleton remodelling: role of gelsolin and cooperation with the MAPK signalling pathway. *J Cell Sci*. 2006;119(pt 10):2156–2167.
82. Ostenson CG, Gaisano H, Sheu L, Tibell A, Bartfai T. Impaired gene and protein expression of exocytotic soluble N-ethylmaleimide attachment protein receptor complex proteins in pancreatic islets of type 2 diabetic patients. *Diabetes*. 2006;55(2):435–440.
83. Gaisano HY, Ostenson CG, Sheu L, Wheeler MB, Efendic S. Abnormal expression of pancreatic islet exocytotic soluble N-ethylmaleimide-sensitive factor attachment protein receptors in Goto-Kakizaki rats is partially restored by phlorizin treatment and accentuated by high glucose treatment. *Endocrinology*. 2002;143(11):4218–4226.
84. Ostenson CG, Chen J, Sheu L, Gaisano HY. Effects of palmitate on insulin secretion and exocytotic proteins in islets of diabetic Goto-Kakizaki rats. *Pancreas*. 2007;34(3):359–363.
85. Lanzetti L. Actin in membrane trafficking. *Curr Opin Cell Biol*. 2007;19(4):453–458.
86. Malacombe M, Bader MF, Gasman S. Exocytosis in neuroendocrine cells: new tasks for actin. *Biochim Biophys Acta*. 2006;1763(11):1175–1183.
87. Porat-Shliom N, Milberg O, Masedunskas A, Weigert R. Multiple roles for the actin cytoskeleton during regulated exocytosis. *Cell Mol Life Sci*. 2013;70(12):2099–2121.
88. Gu C, et al. Direct dynamin-actin interactions regulate the actin cytoskeleton. *EMBO J*. 2010;29(21):3593–3606.
89. Tanabe K, Takei K. Dynamic instability of microtubules requires dynamin 2 and is impaired in a Charcot-Marie-Tooth mutant. *J Cell Biol*. 2009;185(6):939–948.
90. McNiven MA, Kim L, Krueger EW, Orth JD, Cao H, Wong TW. Regulated interactions between dynamin and the actin-binding protein cortactin modulate cell shape. *J Cell Biol*. 2000;151(1):187–198.
91. Lee E, De Camilli P. Dynamin at actin tails. *Proc Natl Acad Sci U S A*. 2002;99(1):161–166.
92. Orth JD, McNiven MA. Dynamin at the actin-membrane interface. *Curr Opin Cell Biol*. 2003;15(1):31–39.
93. Shen H, et al. Constitutive activated Cdc42-associated kinase (Ack) phosphorylation at arrested endocytic clathrin-coated pits of cells that lack dynamin. *Mol Biol Cell*. 2011;22(4):493–502.
94. Poulsen F, Jensen KB. A luminescent oxygen channeling immunoassay for the determination of insulin in human plasma. *J Biomol Screen*. 2007;12(2):240–247.
95. Lou X, Scheuss V, Schneggenburger R. Allosteric modulation of the presynaptic Ca^{2+} sensor for vesicle fusion. *Nature*. 2005;435(7041):497–501.